Measuring Dispersal and Tracking of Anti-Icing and Deicing Chemicals by Using In-Situ Spectral Data – Phase I

FINAL PROJECT REPORT

by

Nathan Belz | University of Alaska Fairbanks
Gabriel Fulton | University of Alaska Fairbanks

Sponsorship
PacTrans, University of Alaska Fairbanks, AKDOT&PF

for
Pacific Northwest Transportation Consortium (PacTrans)
USDOT University Transportation Center for Federal Region 10
University of Washington
More Hall 112, Box 352700
Seattle, WA 98195-2700

In cooperation with US Department of Transportation- Office of the Assistant Secretary for Research and Technology (OST-R)

DISCLAIMER

The contents of this report reflect the views of the authors, who are responsible for the facts and the accuracy of the information presented herein. This document is disseminated under the sponsorship of the U.S. Department of Transportation's University Transportation Centers Program, in the interest of information exchange. The Pacific Northwest Transportation Consortium, the U.S. Government and OSU, UI, UAF, UW, and WSU assume no liability for the contents or use thereof.

Technical Report Documentation Page

1. Report No.	2. Government Accession No.	3. Recipient's Catalog No.	
	01701498		
4. Title and Subtitle Measuring Dispersal and Tracking of Anti-Icing and Deicing Chemicals by Using In-Situ Spectral Data – Phase I		**5. Report Date** **6. Performing Organization Code** G00010259	
7. Author(s) Nathan Belz | University of Alaska Fairbanks 0000-0003-0814-110X Gabriel Fulton | University of Alaska Fairbanks		**8. Performing Organization Report No.** 2017-S-UAF-2	
9. Performing Organization Name and Address PacTrans Pacific Northwest Transportation Consortium University Transportation Center for Region 10 University of Washington More Hall 112 Seattle, WA 98195-2700		**10. Work Unit No. (TRAIS)** **11. Contract or Grant No.** 69A3551747110	
12. Sponsoring Organization Name and Address United States of America Department of Transportation Research and Innovative Technology Administration		**13. Type of Report and Period Covered** Final Report Research Applied **14. Sponsoring Agency Code**	
15. Supplementary Notes Report uploaded at www.pacTrans.org			

16. Abstract

Snow and ice accumulation on pavement reduces roadway surface friction, resulting in diminished vehicle maneuverability, slower travel speeds, reduced roadway capacity, and increased crash risk. Though the use of chlorides and other freeze-inhibiting substances have been shown to reduce these negative factors, methods to quantify and analyze snow and ice remediation methods, as well as the imposed loss of material, are needed to allow state and municipal agencies to better allocate winter maintenance resources and funding. The use and application of chlorides, sand, and their related mixtures and derivatives have proved to be highly effective for controlling or removing the development of ice on the roadway surface. Yet if the amount of salt in solution becomes too dilute, then it no longer retains the capacity to control the development of, or to melt, ice on the roadway and may prove to be more detrimental by allowing the previously melted material to refreeze with a smoother (i.e., more slippery) surface state. An automated and efficient method to quantify the amount of imposed loss of anti-icing and deicing materials has yet to be established. The goal of Phase 1 of this project was to determine to what extent winter roadway surfaces can be analyzed by using spectrometry to determine the coverage and longevity of various types of applications in a laboratory setting. By using a systematically paired analysis of changes in spectrometric curves as solution concentrations changed, relationships were generated that detected changes in deicing and anti-icing compounds reliably.

17. Key Words		18. Distribution Statement	
Winter maintenance, remote sensing, spectrometry, anti-icing, deicing		No restrictions.	
19. Security Classification (of this report)	**20. Security Classification (of this page)**	**21. No. of Pages**	**22. Price**
Unclassified.	Unclassified.	88	N/A

Form DOT F 1700.7 (8-72) **Reproduction of completed page authorized**

TABLE OF CONTENTS

List of Figures

List of Tables

List of Abbreviations

AK	Alaska
AKDOT&PF	Alaska Department of Transportation and Public Facilities
Band Math	Mathematical Comparison of Wavelengths
$CaCl_2$	Calcium chloride
CMA	Calcium Magnesium Acetate
FHWA	Federal Highway Administration
HyLab	Hyperspectral Imaging Laboratory
KAc	Potassium Acetate
MDSS	Maintenance Decision Support System
$MgCl_2$	Magnesium chloride
NaCl	Sodium Chloride
NDVI	Normalized Difference Vegetation Index
NIR	Near infrared
NUV	Near ultraviolet
PNS	Pacific Northwest Snowfighters
PSR+	PSR+ 3500 Spectroradiometer
RWIS	Road Weather Information Systems
USDOT	United States Department of Transportation
VIS	Visible

Acknowledgments

This work has been funded by the US Department of Transportation's University Transportation Center Program, Grant # 69A3551747110, through the Pacific Northwest Regional University Transportation Center and with in-kind match from the Alaska Department of Transportation and Public Facilities Northern Region Maintenance Division. The authors would like to thank the PacTrans Regional University Transportation Center for its generous financial and administrative support of this project. This study would also not have been successful without the significant contributions from the University of Alaska Fairbanks HyLab, Dr. Anupma Prakash, and Dr. Franz Meyer.

Chapter 1. Introduction

1.1 Problem Statement

Over 70 percent of roads in the United States are located in cold and snowy regions (Federal Highway Administration, 2017). The management of anti-icing and deicing efforts during winter months in these regions is critical for mobility and safety. Snow and ice accumulation on pavement reduces roadway surface friction, resulting in lower vehicle maneuverability, slower travel speeds, reduced roadway capacity, and increased crash risk. The extent to which certain chemicals and practices are effective at mitigating the effects of snow and ice are, for the most part, well understood. However, little knowledge exists on the physical processes that affect the longevity of these applications. Methods to quantify and analyze snow and ice remediation methods, as well as the imposed loss of material, are needed. This information would allow state and municipal agencies to better allocate resources and funding for winter maintenance efforts.

1.2 Background

The use and application of salt, sand, and their related mixtures and derivatives have proved to be highly effective for controlling or removing the development of ice on the roadway surface. Ample research exists to indicate the way in which application method, application rate and efficacy of mix contents can vary depending on temperature and surface conditions. There is also substantial research on the environmental impacts of anti-icing and deicing applications on factors such as soil and groundwater, as well as the corrosive properties of different types of chlorides. However, little if any research has quantified the longevity and dispersal of anti-icing and deicing compounds after they have been applied to the roadway surface (i.e., how long does it stay in place and where does it go after it has been applied?). It stands to reason that anti-icing and deicing compounds (e.g., salt and sand) are only effective at or above a certain

concentration. That is to say, if the amount of salt in solution becomes too dilute, then it no longer retains the capacity to control the development of, or to melt, ice on the roadway and may prove to be more detrimental by allowing the previously melted material to refreeze. The different methods for salt to be transported away from the location of application are demonstrated in figure 1.1. These include tracking due to mechanical movement by vehicles, lateral dispersion due to mechanical movement by vehicles or flow of water from melting ice and snow, aerosolization of applied material through the application process or mechanical movement, and adherence to vehicles and deposition elsewhere.

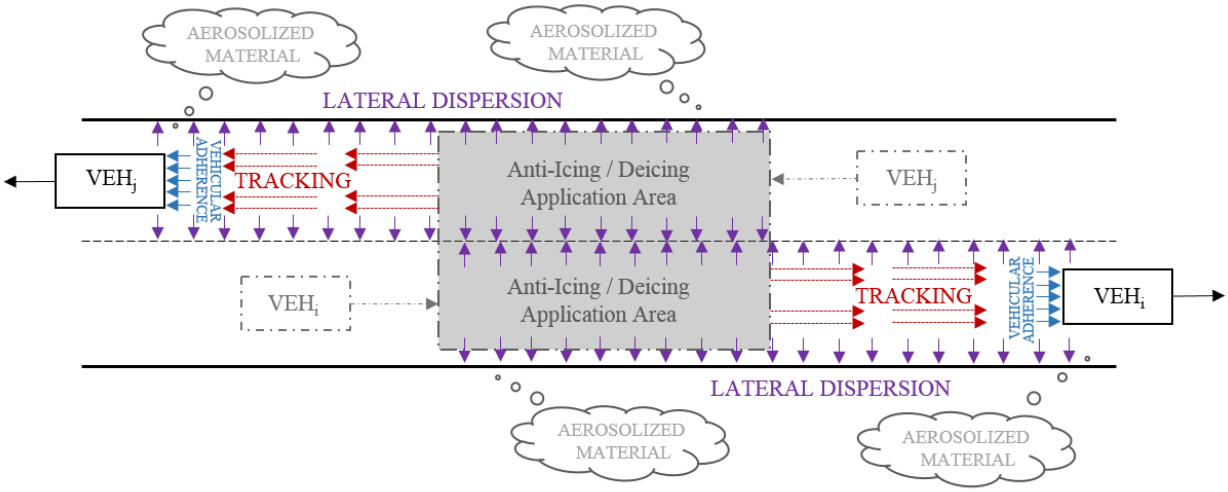

Figure 1.1. Methods of anti-icing/deicing migration/transport

Objectives

The goal of this project was to determine to what extent winter roadway surfaces can be analyzed with spectrometry in a lab setting to record the percentage of reflectance at each wavelength and how reflectance changes with dilution or film thickness. The results and deliverables of this research demonstrate the broader applicability of spectral sensing technologies in the field of transportation. The findings of this research also serve to quantify the effects on visible and infrared reflectance of anti-icing and deicing chemicals and may provide

information that can be used to better inform winter maintenance efforts and activities. Three degrees of detection were attempted:

1) the presence versus non-presence of chemical;
2) the percentage of surface coverage within the viewshed of the spectral unit; and
3) the concentration of deicer present.

Chapter 2. Literature Review

There are roughly 4 million miles of roads and streets in the United States with more than 135 million registered motor vehicles. Over 70 percent of these roads are located in snowy regions, which the Federal Highway Administration (FHWA) classifies as locations that receive more than 5 inches of average snowfall annually (FHWA, 2017a). The accumulation of snow and ice on roads lowers pavement surface friction, causing reduced vehicle maneuverability, slower travel speeds, reduced roadway capacity, and increased crash risk. Because of the negative effects of seasonal winter conditions on driving, fighting snow and ice is a priority for organizations tasked with the maintenance of public roads and highways (e.g., city and state maintenance divisions). The risks associated with winter roadway conditions are immediately apparent to the average motorist who has driven on icy or snow-covered roads. Reduced friction caused by ice and snow (and to some extent colder pavement conditions and colder tire rubber) leads to increased accident rates, increased time to accelerate or come to a stop, and reduced visibility. The problem is that these effects may not be visually apparent to a driver. In order to understand the restrictions imposed by winter roadway conditions, the effects must be quantified.

2.1 Costs of Snow and Ice Accumulation

Roadway speeds can be reduced by up to 40 percent on snowy or slushy pavement (FHWA, 2017a). Reduced traffic speeds, while impactful on the average motor vehicle operator, are not the biggest risk associated with snow and ice. Of most concern is the prevalence and risk of crashes. Of the crashes reported to the FHWA in the last 10 years, on average 1,234,145 weather-related crashes occurred per year, which could be further broken down as 18 percent in snow/sleet, 13 percent on icy pavement, and 16 percent on snow/slushy pavement (Federal Highway Administration, 2017b).

From a public safety perspective, managing snow and ice accumulation is a critical step in the prevention of such weather-related accidents. The costs associated with managing snow and ice accumulation can be significant. Winter road maintenance accounts for roughly 20 percent of DOT maintenance budgets, totaling almost 2.3 billion dollars annually (Federal Highway Administration, 2017). Perhaps more so than any other state in the nation, Alaska must deal with considerable snowfall and the longest periods of sub-zero temperatures, and by extension Alaska also has the coldest air and pavement temperatures. Alaska has 5,600 miles of state-owned roadways, 845 bridges, and 79 maintenance facilities located in areas that can see climatic conditions that range from 100 degrees Fahrenheit to -80 degrees Fahrenheit and snowfall accumulation totals as high as 974 inches in a single year (Monteleone, 2012).

The Central Region division of the Alaska Department of Transportation and Public Facilities (Alaska DOT&PF) and the city of Anchorage spent $16 million on snow maintenance in the winter of 2011 (Roads & Bridges, 2017). These costs may seem astronomical for fighting snow and ice; however, a study done by IHS Global Insight attempted to quantify the economic impact of a one-day, snow-related shutdown. Researchers estimated that a one-day shutdown for a state would cost $300-700 million for businesses, governments, and people, and that snow-related shutdowns would harm hourly workers the worst, accounting for two thirds of direct economic losses (IHS, 2014). Clearly, the economic impact of snow-related closures far exceeds the cost of snow removal and control.

2.2 Snow and Ice Remediation Applications

Instead of physically or mechanically removing snow and ice from roads, chemical-based remediation methods can be used. Many materials can be applied to roadway surfaces by winter maintenance crews to make roads safer for motorists. Chemicals, such as chlorides and other salt derivatives, can be applied to melt the ice by lowering the temperature at which ice forms. These

salts can have admixtures added to them in the form of different carbohydrates that can further enhance their efficacy, such as beet juice. Dry abrasives, such as gravel or sand, can also be applied to add traction to icy roads. Applying these different materials can drastically increase safety on roads by increasing the traction of road surfaces and, if used appropriately, without too much associated cost.

Chemical removal of ice and snow is most commonly achieved by using chlorides and is facilitated by physical application as a solid or dissolved in water to form a liquid brine. The three most widely used snow and ice control salts are sodium chloride (NaCl), magnesium chloride ($MgCl_2$), and calcium chloride ($CaCl_2$) (Fay et al., 2008). The goal of applying these chlorides to a roadway surface is to lower the freezing point of water. By reducing the freezing point of water, the accumulation of ice can be avoided, and the bond between ice and the pavement surface can be released. The deicer that is best suited for a given region, city, or winter maintenance crew is determined through many factors, such as melting capacity, temperature performance, environmental impacts, corrosion impacts, and consistency issues. The effects of the five most common deicing chemicals on the freezing point of water are shown in figure 2.1. The effects of deicing chlorides can be improved with additives such as carbohydrates.

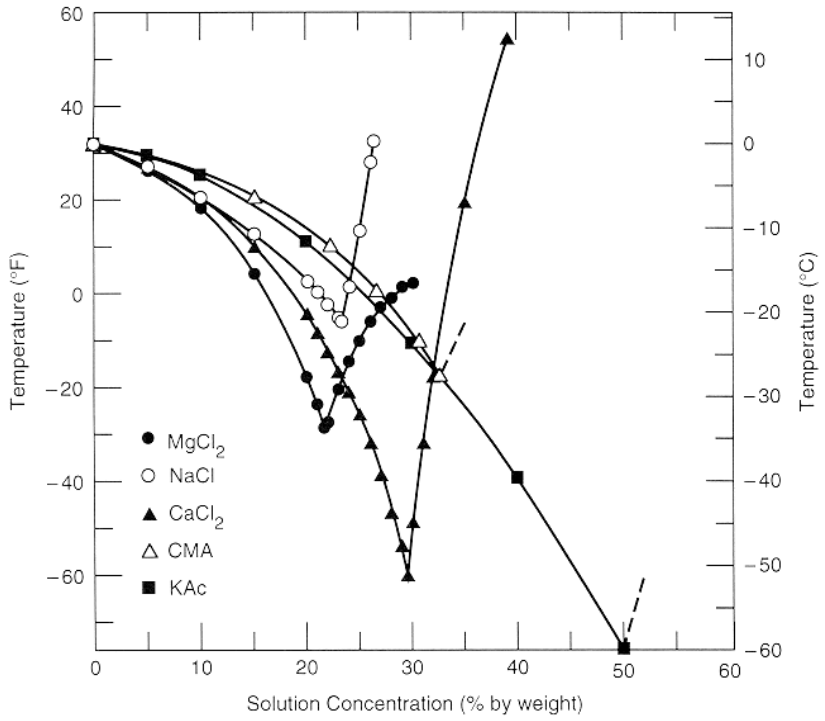

Figure 2.1. Relative temperature of efficacy by concentration for chemical deicers (FHWA, 1996)

For most deicing compounds, the freezing point temperature decreases as the concentration of the respective chemical increases. This relationship holds true until a temperature known as the *eutectic point,* at which the freezing temperature subsequently increases. Falling below the deicer temperature curves means the solution has frozen, and only a mixture of solids and ice will remain. Practically speaking, when applying deicing compounds, winter maintenance crews strive to achieve a concentration as near to, but not exceeding, the eutectic point as possible. Conversely, it is important that the concentration does not fall to such a low point that freezing can occur. Balancing the concentration of deicer has profound implications for determining the likely performance of an ice-control product on the road. Factors that must be considered when deicing compounds are used include not only the quantity of snow or ice that a product can melt, but also the rate at which they melt, how long it will be

before the melted ice and remaining deicer will refreeze, and how much winter events or repeated motorist passage will spread the deicer off of the road (Nixon et al., 2007).

Calcium magnesium acetate (CMA) and potassium acetate (KAc) both need significantly higher concentrations than sodium chloride in order to remain effective (see figure 2.1). Because of this reduced melting capacity, calcium magnesium acetate and potassium acetate conservatively need 1.4 times the concentration to equal the temperature performance of sodium chloride. Higher volumes require more operator time to transport and apply and therefore have considerably higher costs per application treatment (FHWA, 1996).

However, chemical deicers have operational, environmental, and infrastructural drawbacks. One of the main operational concerns about the application of deicing liquids on highways is the potential for the deicer to create a slick surface. One of the causes of slickness associated with deicers occurs when the chloride liquid dries out and leaves a chemical slurry that reduces road surface friction (Nixon et al., 2007). Winter maintenance crews can avoid this effect by not applying chemicals to the road surface when temperatures are above 40 degrees Fahrenheit.

All deicing compounds that are placed on roads will eventually be transported away from the road and end up in nearby soils, then enter storm drains, and ultimately reside somewhere in the surrounding environment. It is the responsibility of those applying these compounds to consider the deleterious effects of these substances. Excessive use of deicing compounds has the potential to negatively affect the environment. Damage to the environment should be weighed against the benefits such as reducing vehicle accidents (e.g., a car crash), which can also create environmental damage in the forms of leaked gasoline, oil, and coolant that may disperse far from the scene of a crash. The Pacific Northwest Snowfighters (PNS) requires that toxicity tests

be run on deicing compounds, including the Rainbow Trout or Flathead Minnow Toxicity Test, Ceriodaphnia Dubia Reproductive and Survival Bioassay, and Selenastrum Capricornutum Algal Growth test, whose procedures are described by the EPA and American Public Health Association (1976) (Nixon et al., 2007).

Water quality, air quality, soil quality, and land- and water-based plants and animals can be negatively affected by deicers. A study done by the USGS Wisconsin Water Science Center investigated the effects of deicer material runoff on aquatic toxicity surrounding an airfield and found that chloride and sodium analyses demonstrated the influence of urban runoff on the nearby watershed, especially downstream from the airport, where concentrations of these road-salt-derived contaminants increased because of salting of roads, parking lots, and sidewalks downstream from airport drainage (Corsi et al., 2008). Between November 1996 and April 2007, 47 samples were collected to check for chlorides. The study found that 68 percent of samples exceeded the hourly average USEPA water-quality criterion (860 mg/L), and 91 percent of samples exceeded the four-day average criterion (230 mg/L). The authors concluded that salt runoff from roads had a considerable effect on aquatic life in the watershed near the tested airport (Corsi et al., 2008). A study prepared for the Illinois Department of Transportation by the Atmospheric Environment Section of the Illinois State Water Survey tested the atmospheric dispersion of deicing salt through aerosolization. The data were collected with continuous, high volume aerosol samplers, a dichotomous aerosol sampler, and through collection of snow samples at different distances from Interstate 55 (Williams et al., 2000). The results were that the salt deposition pattern near a treated roadway, as determined by snow samples, decreased consistently with distance from a road. The average deposition per length of a roadway was 300 pounds per mile which was similar to the Illinois Department of Transportation's typical salt

application in 1994 (Williams et al., 2000). The authors concluded that no source of aerosolized deicer material could be determined from the research done so far, but confirmed that indeed deicer is dispersed into the area surrounding the sides of the road. This suggests the need for additional studies on detection and tracking of deicing materials and was one of the motivating factors for the research presented herein.

Deicer products have the potential to damage many aspects of the transportation infrastructure, such as pavement, rebar, metals, roadside equipment, and vehicles. Deicers can affect concrete both physically and chemically. Physical effects are typically manifested as cracking and scaling. The chemical effects result from reactions involving hydration products, aggregates, or corrosion of the reinforcing steel (Sumsion & Guthrie, 2013). The deicer ions react chemically with concrete and leach calcium hydroxide from the paste, decalcify the calcium silicate hydrate, convert the magnesium silicate hydrate, and form brucite, complex salts, and oxychlorides. An alkali-silica reaction and alkali-carbonate reaction can be initiated and accelerated by alkalis from deicers, and the accumulation of critical concentrations of chloride ions around steel can initiate corrosion (Sumsion & Guthrie, 2013). Using information gathered by various sources, the Utah Department of Transportation concluded that sodium chloride should be utilized by engineers responsible for winter maintenance wherever possible instead of CaCl, $MgCl_2$, and CMA, and they should utilize only the amount needed to ensure the safety of the traveling public (Sumsion & Guthrie, 2013). Use of deicers, in most amounts, can be damaging to vehicles and the infrastructure on which they travel. However, using deicing compounds such as sodium chloride can be extremely beneficial to ensure safe winter roadways.

One option other than chlorides and chemicals are sands and gravels. These abrasives provide temporary but immediate traction on icy roads. Abrasives are most effective for vehicles

traveling 30 mph or less. If vehicles are traveling faster than 30 mph, there are diminishing returns on traction and additional costs related to clean-up (National Academies of Sciences, Engineering, and Medicine, 2007). Consequently, the most effective places for abrasives to be applied are on low volume roads near hills, curves, and intersections where speeds are relatively low. Yet, the use of abrasives may also be warranted when other ice remediation methods are less effective. One of the key problems with applying abrasives is that they do not easily stay on the road. Repeated wear and tracking from passing vehicles cause loose abrasives to migrate, spreading along the roadway and off the sides of the road. If another snowfall event occurs, much of the abrasives will be plowed or blown away. Without enough abrasives present, their effectiveness will be greatly reduced and reapplication will be necessary. To prevent scatter and ensure that the abrasives will remain on the roadway surface as long as possible, three general approaches can be used: pre-wetting sand with liquid deicers, pre-wetting sand with hot water at 30 percent by weight mix, or heating sand to 356 degrees Fahrenheit (Vaa, 2004; Staples et al., 2004; Lysbakken and Stotterud, 2006; Ontario Ministry of Transportation, 2008; CTC & Associates, 2008). These methods effectively cause the ice surrounding the abrasive to partially melt, allowing the abrasive to penetrate the surrounding ice, which upon freezing locks the abrasive in place.

2.3 Information Assistance Systems

In addition to applying materials to roadways, information gathering techniques can also aid in making winter roadways safer for motorists and help maintenance operations make better and more informed decisions. Equipment devoted to gathering information for the DOT are known as Road Weather Information Systems (RWIS). These stations provide real-time weather data: air temperature, humidity, visibility distance, wind speed, precipitation type and rate, cloud cover, and air quality. RWIS stations also measure roadway data such as pavement temperature,

freezing point, roadway condition, and soil temperature. An Alberta Infrastructure and Transportation (2006) project cited by Clear Roads studied the pros and cons of utilizing RWIS and anticipated that RWIS would deliver $5.38 in benefits for every dollar spent (e.g., more efficient use of winter maintenance equipment and deicing chemicals, reduced rate of vehicle collisions, and reduced labor costs). A survey conducted by Clear Roads indicated that of the organizations that had implemented weather forecasting systems, 90 percent indicated having improved or expanded upon current systems, and 77 percent indicated having expanded their RWIS or weather station networks (Fay et al., 2015). The survey provided evidence that weather and pavement information systems are becoming more widely used for winter maintenance operations. RWIS stations can be used in conjunction with a Maintenance Decision Support Systems (MDSS). The MDSS assists maintenance personnel in determining roadway maintenance activities by providing real-time and post-storm analysis to evaluate materials used, rate of application, and timing of application (Fay et al., 2015). A study conducted in Indiana found that by using MDSS, the salt savings in the winter of 2008 were about 228,470 tons ($12,108,910), and if normalized for winter conditions based on storm severity, the total salt savings were 188,274 tons ($9,978,536) (McClellan et al., 2009). Reducing salt usage while also maintaining safe roads is a keen interest of those who utilize it for winter maintenance purposes. The benefits of information gathering and processing are demonstrated by increased safety and cost savings.

2.4 Spectrometry and Applications to Detect Deicers

The research presented here sought to apply spectrometry and related methodologies to detect elements of deicers. Hyperspectral imaging is a form of remote sensing that quantifies the reflectance of a target surface. Remote sensing methods are advantageous because they negate the need for physically sampling or, depending on the method of data collection, physically

occupying areas that would be unsafe, untimely, or otherwise inaccessible. Spectral imaging can take many forms, from physical contact reading in which the device must be pressed against a surface, to field units capable of distances of up to several feet, to drone and airplane mounted devices, to units housed in satellites.

Spectral analysis often requires the use of "band math," which is a form of mathematical analysis used to interpret reflectance spectra gathered from spectral imaging units. A reflectance spectra records specified wavelengths and their corresponding reflectance values. Band math compares the relative amount of reflectance at one wavelength to the amount at other wavelengths. Depending on which wavelengths are available, a number of mathematical ratios and comparisons can be employed to gather information and make assumptions. One of the most well-known band math equations is the Normalized Difference Vegetation Index (NDVI), which is used to analyze vegetation. The NDVI looks at the ratio of near infrared (NIR) and red bands [(NIR-RED)/(NIR+RED)], and the resulting values can be interpreted to determine vegetation health (Schuckman, n.d.). NDVI analysis was developed and works because of the knowledge about the materials being analyzed. Healthy vegetation reflects more NIR and green light than other wavelengths; conversely, healthy vegetation absorbs more red and blue light. Using NDVI the image in figure 2.2 (a) can be analyzed, and the subsequent result will assign each pixel a value from -1 to 1 in figure 2.2 (b), green representing proximity to NDVI of 1 or healthy vegetation. A value closer to 1 would signify a healthy vegetation; a value closer to 0 would signify unhealthy vegetation. A negative value would indicate the presence of water, since water is highly absorptive of NIR. Other forms of band math can be used and depend on the inherent reflectance of the surfaces and materials being analyzed.

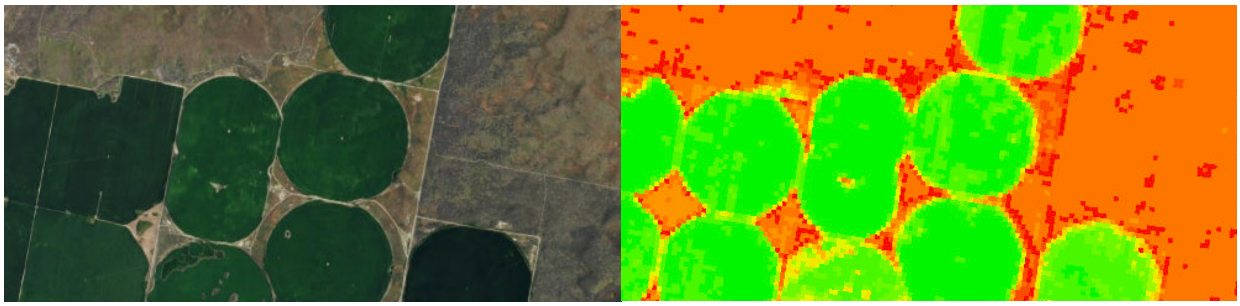

Figure 2.2 (a) Pre NDVI processing (b) Post NDVI processing (GIS Geography, 2018)

Reflectance analyses like these are particularly useful for monitoring temporal trends in phenomena of interest. For example, NDVI is useful for farmers monitoring locations where vegetation is most healthy versus least healthy for future agricultural management. NDVI can also be applied to monitoring forest fires and the resulting burn scars. The possibilities and applications of spectrometry are growing and research continues to show, such as the study presented herein, the broad applications of spectrometry.

2.5 Conclusion / Research Need

As new ways to measure, process, and plan for winter storm events emerge, new efficiencies in the forms of cost savings, environmental protection, or safety can be discovered. The research presented herein attempted to utilize existing methods in spectrometry to track dispersal and concentrations of deicers. On the basis of the recorded reflectance and adsorption peaks that are unique to substances, materials can be identified and cataloged. For example, chloride and sodium molecules have specific wavelength peaks and can be identified when water and sodium chloride are compared in aqueous solution. The specific application presented here was the application of wavelength analysis to monitor the dispersal and transport of deicer (e.g., surface concentrations, surface coverage, and migration).

Ideally, this research will lead to the development of integrated spectrometer units that can be collocated with RWIS stations, thus allowing them to be used in conjunction with a Maintenance Decision Support Systems (MDSS). The MDSS assists maintenance personnel in

the decision-making processes of determining roadway maintenance activities by providing real-time and post-storm analysis to evaluate materials used, rate of application, and timing of application (Fay et al.,2015). Because of the large savings reductions possible, as discussed previously, reducing salt usage while also maintaining safe roads is a keen interest of those who utilize it for winter maintenance purposes. The benefits of information gathering and processing are demonstrated by increased safety and cost savings.

Chapter 3. Spectral Data and Methods

3.1 Labratory Preparation

This research employed the use of facilities and equipment available through the University of Alaska Fairbanks (UAF) Hylab, specifically the spectral imaging unit instrumentation (e.g., HySpex VNIR-1800 and SWIR-384 pushbroom HS cameras). The Hylab has an ASD Fieldspec and a PSR+ 3500, which can be used for field and lab based measurements and has accessories for calibration, normalization, and analysis. The PSR+ 3500 hyperspectrometer ranges from 350 nm to 2500 nm wavelengths, which encompasses the near infrared, visual, and near ultraviolet wavelengths. To maximize the accuracy and consistency of data recorded by the PSR+ 3500, the UAF Hyperspectral Imaging Laboratory has a halogen lamp (figure 3.1a) that mimics the spectrum and consistency of intensity that natural sunlight outputs (figure 3.1b).

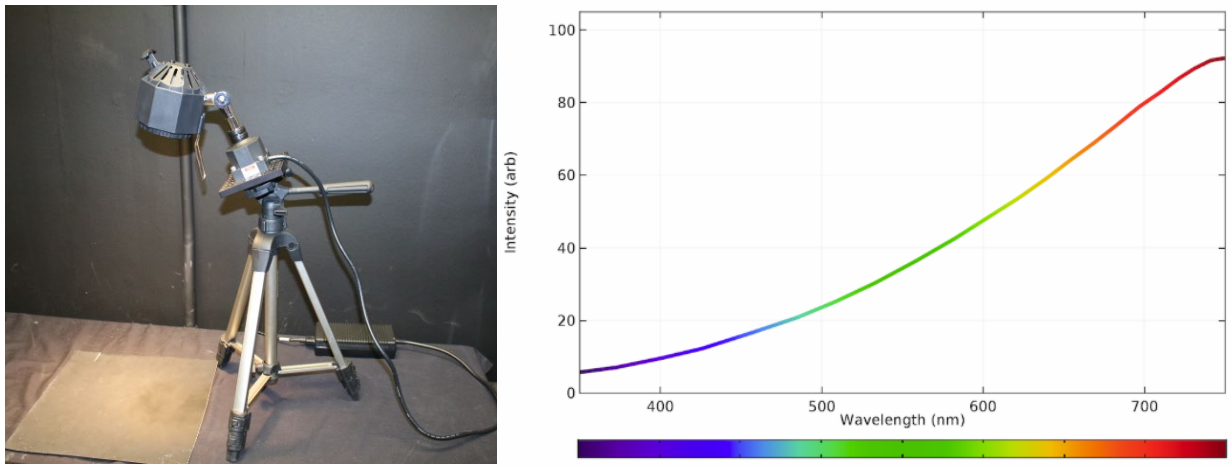

(a) (b)

Figure 3.1 (a) Halogen lamp in the UAF Hylab (b) Halogen lamp spectra (*Illumination*, n.d.)

The natural sunlight spectrum (figure 3.2) can be compared to the halogens' spectrum; both curves have complete coverage of the wavelengths, unlike most sources of light.

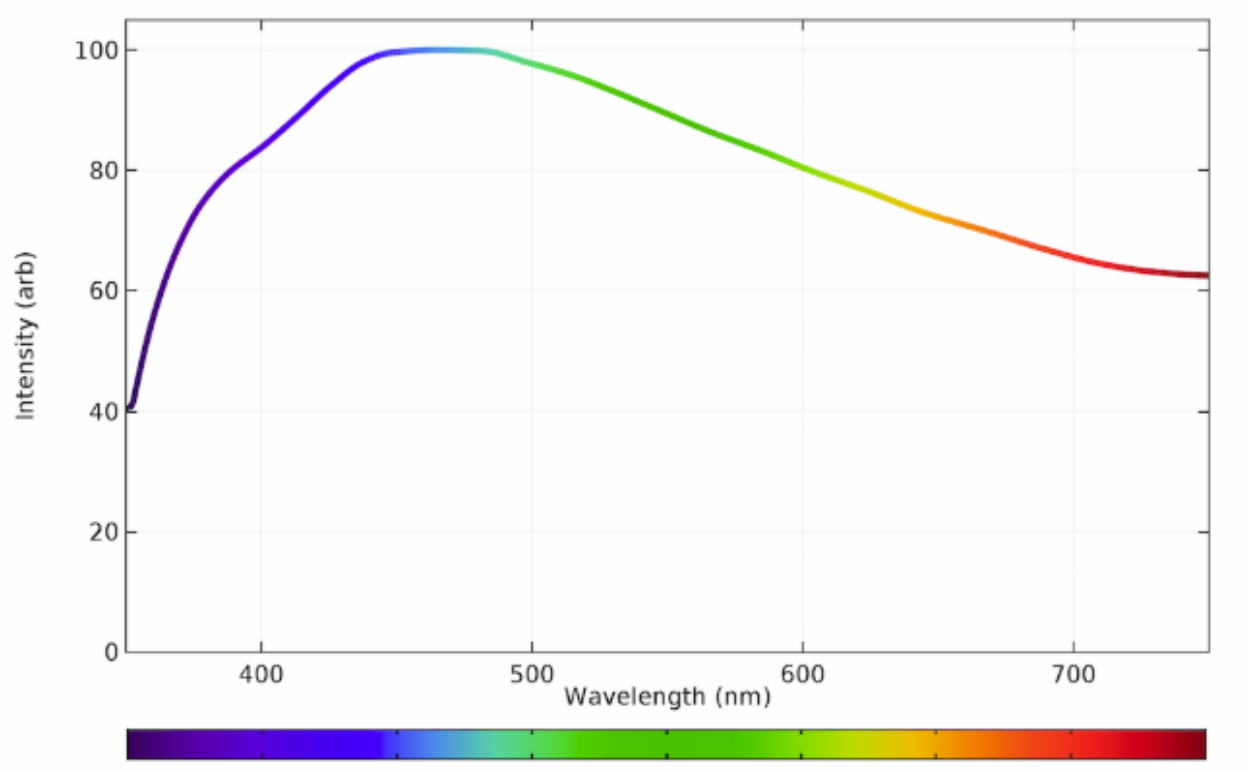

Figure 3.2 Sunlight spectra (*Illumination*, n.d.)

The PSR+ 3500 collects the reflectance of surfaces in the wavelength range of 350 to 2500 nm. The walls, ceilings, and surfaces of the lab are either painted in black paint or covered in black material to minimize extraneous scatter or reflectance. The imaging background is a specially painted black matte board with a flat reflectance spectrum. Extraneous light from outside of the lab is eliminated by restricting access to the lab during imaging. Occupancy of the spectral lab is indicated by closing the door to the small testing room and by turning off the lights in the adjoining room. Light emitted from LED (figure 3.3a) and fluorescent tube (figure 3.3b) lights do not have a continuous spectrum like natural sunlight or halogen lamps. If some sections of wavelength do not have any illumination, or if there are sporadic peaks, the reflectance of a target surface can be inaccurate (*Illumination*, n.d.).

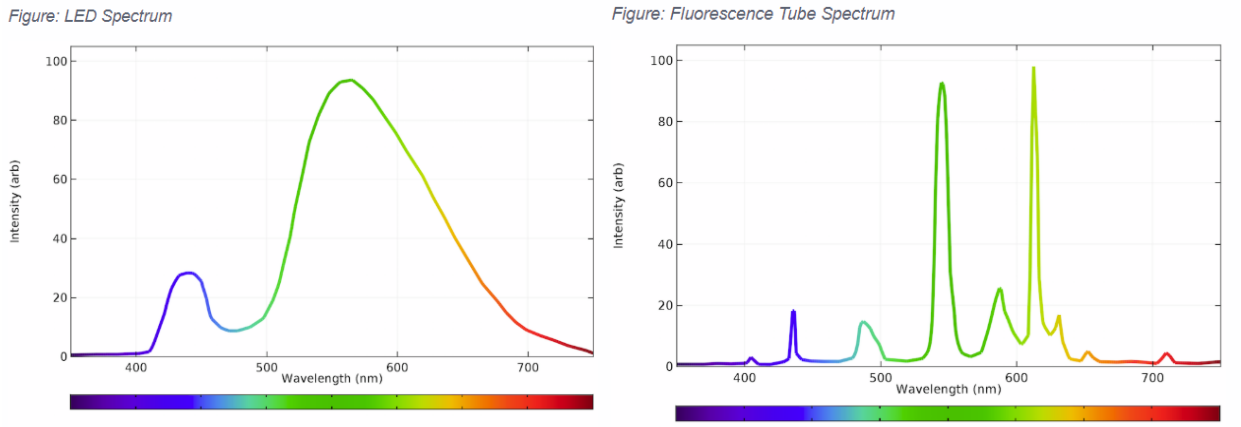

(a) (b)

Figure 3.3 (a) LED spectra and (b) Fluorescent tube spectra (*Illumination*, n.d.)

3.2 Lab Sample Preparation

Samples were generated in the lab to simulate the field conditions of different concentrations of a deicer brine and a deicer beet-brine mixture. These samples went through several iterations as the testing procedures were refined. The first set of data was a proof of concept and comprised the individual components that would normally be found on a roadway during winter remediation. These materials included asphalt pavement, sodium chloride-based rock salt, ice, traction sand, and water. These materials were imaged in the lab and compared to established spectral curves where available.

After the baseline values for the individual components were recorded, permutations and mixtures that would be found in real world situations were explored. Application rates obtained from AKDOT&PF Northern Region are found below in table 3.1. A concentration of 23.3 percent sodium chloride is mixed with a carbohydrate beet juice at an 80:20 ratio.

Table 3.1 AKDOT&PF Northern Region application rates

Pre-wetting sand or salt:	8 to 14 gallons of brine or brine with additive per ton of material
Aggregate:	400-750 pounds per lane mile
Salt:	75-300 pounds per lane mile (condition dependent)
Brine or Brine with additive:	20-30 gallons per lane mile when anti-icing; 30-50 gallons per lane mile when deicing

Variations in the amounts and concentrations of these chloride solutions may vary for several reasons. First, deicing materials applied by AKDOT&PF are not done so ubiquitously and evenly across the transportation network. Key locations such as curves, bridges, bridge approaches, and intersections are typically a higher priority. AKDOT&PF applies brine at a concentration of 23.3 percent, which, as it is designed to do, would slowly melt ice and snow and therefore begin to dilute over time. For lab experimentation, a range of brine solutions was fabricated using tap water and included concentrations at 5 percent, 10 percent, 15 percent, 23.3 percent, and an oversaturated mixture of approximately 40 percent. This set of concentrations encompassed the AKDOT&PF application, as well as subsequent stages of dilution. The oversaturated concentration was used to simulate conditions when either solid salt was applied or evaporation of the ice and snow melt resulted in a high-concentration brine or salt residue. The generated concentrations were fabricated in surface thicknesses of 3.6 mm, 1.6 mm, and 0.8 mm in a petri dish. A film thickness of 0.8 mm was the thinnest achievable thickness in a petri dish. The 3.6-mm film thickness was the first achieved volume added to a petri dish to achieve full surface coverage without mechanical movement of the liquid in the petri dish to reach full coverage. The 1.6-mm film thickness was then chosen as a midpoint for comparison between the 3.6-mm and 0.8-mm film thicknesses. These concentrations were extrapolated and used to prepare a clone of the AKDOT&PF beet mixture (23 percent brine solution mixed with 20 percent beet juice carbohydrate by volume) at different dilutions at surface thicknesses of 3.6

mm, 1.6 mm, and 0.8 mm. Additionally, pure beet juice mixtures were prepared with water and analyzed.

Recording the interactions of the spectral reflectance of these individual components (as they would be present on a roadway surface) was the ultimate goal of this project. However, to control for potential confounding variables, we started by controlling and simulating these field conditions in the lab such that each element could be analyzed individually and then in combination. The simulated winter roadway (figure 3.4) was constructed and housed in a black PVC end cap, which acted as a container for each material layer (i.e., pavement, ice, and brine). An asphalt pavement sample was compacted by using a gyratory compactor in the UAF Asphalt Lab with typical Alaskan roadway specifications. The asphalt pavement sample was then cored to a 3-inch diameter and cut at a thickness that would allow an ice layer to be fabricated on the surface once placed in the PVC cap. The height of the fabricated roadway surface was adjusted in relation to the container rim to reach a desired ice layer thickness by inserting washers underneath the pavement core. Desired volumes of water were applied on the pavement core surface and frozen to create ice layers of varied thicknesses. This simulated road (figure 3.4), was then treated with deicing compounds and/or aggregate at volumes and weights specified by AKDOT&PF.

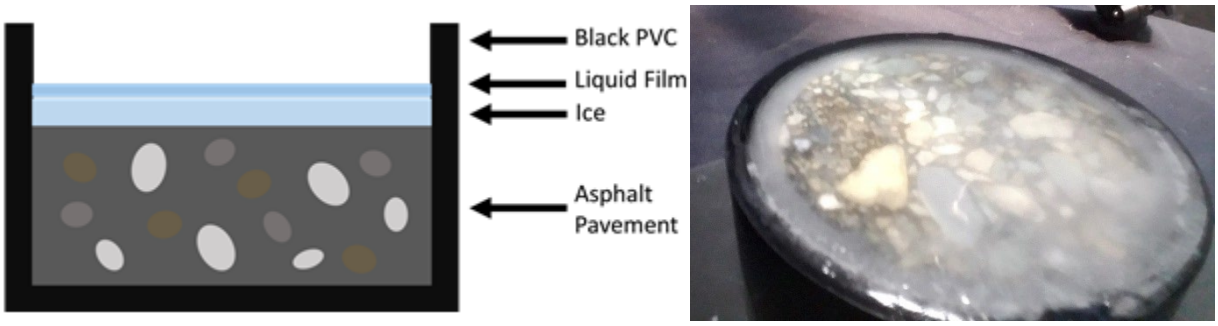

(a) (b)

Figure 3.4 (a) Designed road simulation, (b) Fabricated road simulation

During the initial phase of lab testing it became apparent that ice layer thicknesses, such as those found on regularly treated and maintained roads, were impossible to achieve on the simulated roads. The correct ice thickness could be created; however, ultimately it could not survive the room temperature environments for a long enough time to obtain accurate results with the testing methods in the UAF Hylab. At this stage in the experiment, it was not possible to utilize the spectrometer in the UAF Cold Room laboratory because of the transition between the engineering buildings at UAF from Duckering to ELIF. The thicker the ice layer that was fabricated, the longer it would take for the surface to melt. However, once the ice layer thickness approached 0.4 mm it no longer accurately represented a regularly deiced or maintained roadway. This was not expected to affect the overall experiment because we were primarily concerned with the liquid film above the ice layer, which actually contains the deicing material. Ideally, having a lab background identical to a specified pavement surface type in Alaska would help with calibration issues. Additionally, generating a complete library of all permutations of asphalt- and concrete-based pavements (e.g., levels of wear and aggregate types) would be unrealistic given the scope of this project. However, using the pavement background in the form we were capable was at least a good first step in relating lab results to field conditions.

3.3 Obtaining Lab Data

Setting up the PSR+ spectroradiometer unit began with removing the PSR+ portable spectrometer, white 99 percent reflectance panel, fully charged 7.4V Li-ion battery packs, pistol grip fiber optics holder, and 1.5-meter fiber optic cable from the compact carrying case or storage. The PSR+ unit was then connected to the pistol grip with the fiber optic cable, as shown in figure 3.5.

Figure 3.5. PSR+ spectroradiometer

The halogen lamp had to then be turned on and allowed to warm up for 30 minutes to allow the bulb temperature and emitted wavelengths to stabilize (figure 3.6a). Letting the bulb reach constant temperature ensured that the emitted spectrum would remain constant throughout testing. Before testing a given material with the PSR+ unit, the device had to be referenced to a highly reflective white panel (figure 3.6b), which would adjust the recorded spectra in accordance to lighting conditions currently present.

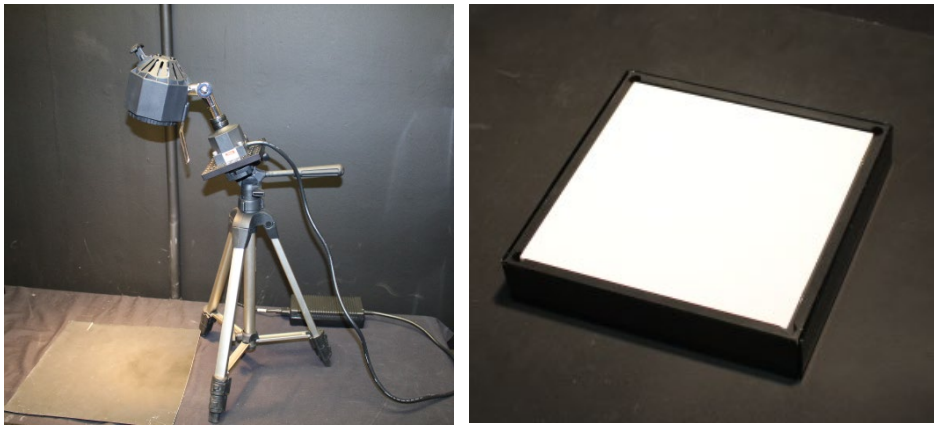

(a) (b)

Figure 3.6 Hylab halogen lamp (a), and white reference panel (b).

The spectroradiometer was then connected to a computer, and the DARWin software was opened. The DARWin software was used to monitor and control data collection (figure 3.7).

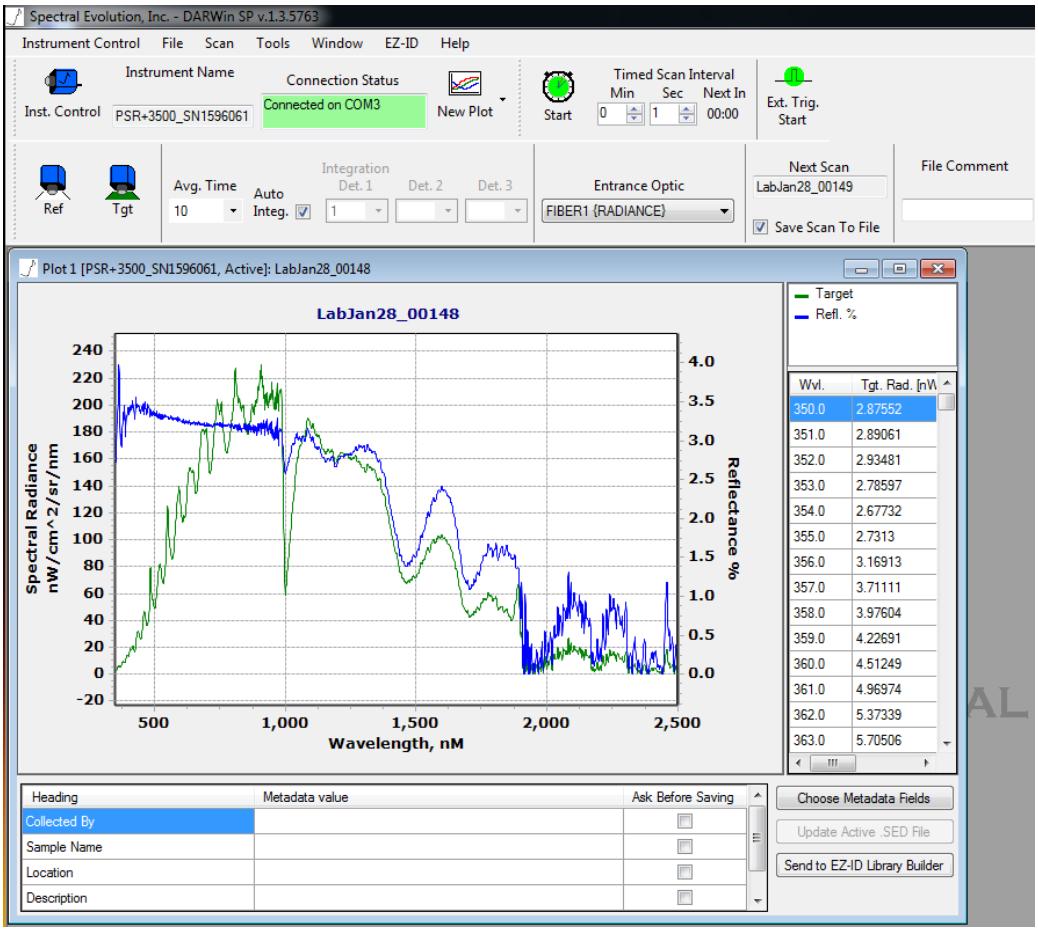

Figure 3.7 DARWin PSR+ Hylab software

The power of the spectroradiometer had to be left to idle for 30 minutes before data collection began. The idling procedure ensured that the unit and fiber optics would remain as constant as possible throughout data collection. The unit could then be made to reference and collect target reflectance on the basis of inputs to DARWin. During the lab testing procedure, the pistol grip was mounted to a tripod for stabilization to expedite the testing procedure. The procedure for lab testing was to reference between every sample material. Ten spectral reflectance curves were obtained for each fabricated lab material used in the relationship analyses presented later in the report.

3.4 Lab Data Collection

The black matte board background used by the Hylab had a consistent reflectance of about 4 percent across all wavelengths. The targeted materials, brine, beet, and beet-brine solutions were placed in petri dishes on top of this constant and non-reflective background. The reflectance of the material was then obtained by using the PSR+ unit, which was pointed at the material orthogonal to the orientation of the material surface. Polystyrene, borosilicate, and flint glass dishes were tested to determine which one would have the best efficacy. The polystyrene dish was deemed to be most advantageous because it allowed the thinnest film thicknesses to be applied. The polystyrene petri dish had a diameter of 88 mm. The thinnest possible film thickness achieved in the polystyrene dish before the water would stick to itself or the rim of the dish was ~0.8 mm or 5 mL of liquid. Anything below 5 mL resulted in incomplete surface coverage; therefore, the minimum thickness value creatable in the lab under these conditions were 0.8 mm. Several other thicknesses were tested, such as 1.6 mm with 10 mL of liquid and 3.6 mm with 22 mL of liquid.

As discussed previously, a range of concentrations was selected that would represent a range of concentrations beginning with the initial application concentration of 23.3 percent down to 0 percent. This would simulate dilution and migration of chemical in a real-world environment. Tested concentrations of brine can be seen in table 3.2. The water used for dilution was the same as that used by AKDOT&PF Northern Region. Additionally, a 40 percent mixture was created past the total dissolution capacity of salt in water to mimic the application of solid salt and the subsequent melt or liquid application that then begins to dry. However, because exact calculation of the percentage was not easily done, it was excluded from the relationship calculations in later R analysis but still included in the early lab work (table 3.2).

Table 3.2 Brine analysis breakdown

Date	Height	Brine Concentration						
24-Jan 2018	3.6 mm	**(%)**	**0**	**5**	**10**	**15**	**23.3**	**~40**
		(mg/cm^2)	0	18.0	36.0	54.0	83.9	144.0
15-Jun 2018	3.6 mm	**(%)**	**-**	**5**	**10**	**15**	**23.3**	**~40**
		(mg/cm^2)	0	18.0	36.0	54.0	83.9	144.0
27-Jun 2018	1.6 mm	**(%)**	**0**	**5**	**10**	**15**	**23.3**	**~40**
		(mg/cm^2)	0.0	8.0	16.0	24.0	37.3	64.0
9-Jul 2018	1.6 mm	**(%)**	**0**	**5**	**10**	**15**	**23.3**	**~40**
		(mg/cm^2)	0.0	8.0	16.0	24.0	37.3	64.0
6-Sep 2018	0.8 mm	**(%)**	**0**	**5**	**10**	**15**	**23.3**	**~40**
		(mg/cm^2)	0.0	4.0	8.0	12.0	18.6	32.0
17-Sep 2018	0.8 mm	**(%)**	**0**	**5**	**10**	**15**	**23.3**	**~40**
		(mg/cm^2)	0.0	4.0	8.0	12.0	18.6	32.0
28-Jan 2019	0.8 mm	**(%)**	**0**	**5**	**10**	**15**	**23.3**	**~40**
		(mg/cm^2)	0.0	4.0	8.0	12.0	18.6	32.0

AKDOT&PF Northern Region also adds 20 percent carbohydrate (i.e., beet juice) to the brine solution to improve the deicing or anti-icing capabilities under certain circumstances. The same NaCl concentrations were used to fabricate lab samples that included beet juice. The levels of beet-brine concentrations generated are shown in fable 3.3.

Table 3.3 Beet-brine analysis breakdown

Lab Date	Height	Beet-Brine Concentrations (%)				
16-Feb 2018	3.6 mm	0	4.3-5	8.6-10	12.9-15	20-23.3
31-May 2018	3.6 mm	-	4.3-5	8.6-10	12.9-15	-
9-Jul 2018	1.6 mm	0	4.3-5	8.6-10	12.9-15	20-23.3
21-Sep 2018	0.8 mm	0	4.3-5	8.6-10	12.9-15	20-23.3
28-Jan 2019	0.8 mm	0	4.3-5	8.6-10	12.9-15	20-23.3

Even though AKDOT&PF does not apply beet juice as an anti-icer or deicer on its own, several concentrations of a beet-only solution were analyzed to identify key absorption features independent of saline concentrations. The spectral signatures of beet and beet-derived solutions do not currently exist, and this would be a significant contribution to the field of spectral imaging. Fabricated concentrations of the beet solutions are given in table 3.4.

Table 3.4 Beet analysis breakdown

Lab Date	Height	Beet Concentration (%)			
16-Feb 2018	3.6 mm	0	10	20	100
8-Jun 2018	3.6 mm	0	10	20	100
9-Jul 2018	1.6 mm	0	10	20	100
21-Sep 2018	0.8 mm	0	10	20	100
28-Jan 2019	0.8 mm	0	10	20	100

These solutions were then added to the fabricated ice-covered road samples to mimic field conditions. However, because of limitations discussed later in the report, the road samples proved to be problematic, and after some experimentation the brine applications were ultimately

discarded from data collection. Each solution was placed in a petri dish, and ten shots of wavelength data were obtained with the PSR+. Data were then averaged into a single curve, and confidence intervals were computed.

3.5 Data Analysis Methods

The first method attempted in the lab to find new relationships was a simple correlation analysis between increasing brine concentrations and the spectral signature of salt. Ideally the absorption points unique to NaCl that affect the liquid brine curve would be highlighted, and as NaCl concentrations increased the correlation to a pure salt signature would also increase. This was ultimately unsuccessful, as the absorption points most relevant to salt lay within the NIR and IR range, which the medium (water) either absorbed completely or, at thinner film thicknesses, obfuscated to the point that it was undetectable with any form of consistency. Therefore, based on the data collected in this research, we concluded that detecting correlations between the NaCl reflectance curve and changing concentrations of brine is not possible while observing the 350- to 2500-nm wavelengths utilizing a PSR+ 3500 field unit.

Band math is the main tool for analyzing spectral reflectance. Depending on ratios and changes in a material, band math can quantify the changes in a measured surface. A computation employed to determine soil salinity for crop health, a salinity index calculated as the square root of ETM+ satellite's Band 3 * Band 4, was the closest example of monitoring salinity in a medium that was found before experimentation was conducted (Asfaw, et al., 2016). The salinity index calculation was tested with lab data; however, no relationship was found. This was suspected to be due to different background types, and therefore a new, unique relationship would need to be created that relied on liquid water as a medium. This project enlisted a method similar to the salinity index and that of the NDVI (see section 2.6 for more discussion) to test correlation, key absorption points, and curve changes for winter roadway deicing materials.

The average wavelength curves were imported into Excel and Rstudio and first visually inspected. If the curves were visually similar when the same solution was repeatedly imaged, then the results were deemed to be free of error, and external effects and could be further analyzed. If the curves appeared to be translated horizontally, had significant shifts in vertical magnitude, or exhibited some other unexpected change, then more scrutiny would be given to results, and retesting would follow to check whether the results were an aberration due to error or to determine the cause.

The process by which the spectra were collated and analyzed evolved as the project advanced. Preliminary procedures involved checking for noise, replication, and consistent identification points such as valley and peak wavelength locations. Computational analysis began with the simplest approaches and branched outward, with new procedures replacing ineffective ones.

A common spectral analysis approach is to identify the local minima and maxima along a spectral curve, often referred to as “peaks” and “valleys.” These peaks and valleys can provide valuable insight on what materials are present or what substances have been added to a material on the basis of shifts and changes in the curve. The reasoning behind this approach is that the local minima and maxima would theoretically be the points most affected by the addition of new materials to an otherwise homogenous materials curve and therefore would be the most sensitive points to monitor for sodium chloride concentration changes. This approach generated the first successful relationships in the research with a linear comparison between two reflectance values on a reflectance curve. However, most of the relationships worked only if the points were offset by 1 to counteract the proximity to 0 reflectance and normalized to isolate changes due to salt content. For the peak and valley analysis of spectra obtained in this study, the local minima and

maxima were first identified by visual inspection. To expedite and automate the process, methods were developed in Excel and Rstudio. These computer generated methods were refined over several iterations to avoid identifying false peaks and valleys generated by noise in the data.

These peaks and valleys in the reflectance curve could be normalized to highlight changes, and the entire curve could be offset to move the lowest reflectance values farther away from 0. The goal of this analysis was to identify a relationship between certain peaks and valleys that would show a trend as salt concentration was increased or decreased. This trend could then ideally be repeated, tested, and extracted, if successful, as a reliable identifier or even measurement of salt presence.

Concerns were raised with limiting the selection of wavelengths to the valleys and peaks of the spectra because of the dampened effects of change, as demonstrated in figure 3.8.

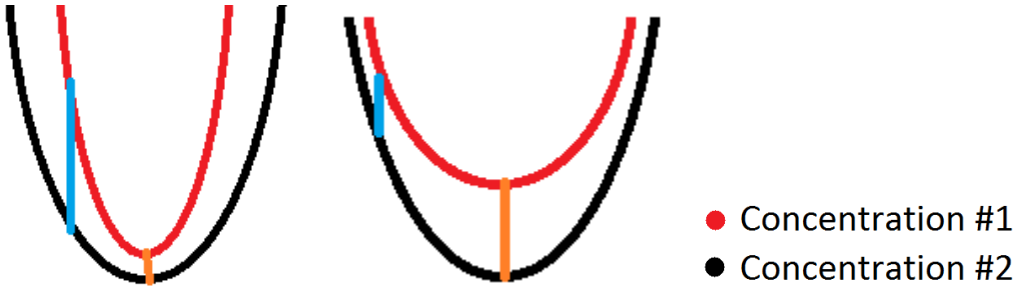

(a) (b)

Figure 3.8 Effects of depression in (a) spectra 1 and (b) spectra 2

If these valleys approached zero or were for some other reason resistive to the absorptive capabilities being added by additional materials, the valleys would not be the best sources for measurement of changes in the spectra. In the figure above the red curve shows a material added to the surface that changes its shape to that of a black curve in two forms of severity. The point of the curve where the orange line touches represents a point of key significance (e.g., a valley on the curve); however, this valley is not located at the point where the greatest change in

reflectance occurs. Rather, wavelength associated with the largest change in reflectance is denoted by the blue line, which is some distance away from the key valley location. This point of actual greatest change in reflectance would be the point at which the reflectance curve should be analyzed.

On the basis of this observation, Rstudio was used to divide each wavelength by every other wavelength, and then the value was compared to the next iteration of concentration (or film thickness). If the values ascended with each iteration, then the wavelength pair would be stored by the program. If the wavelength ratio descended throughout all concentrations, then the wavelength pair would be saved. This program would than collate and organize these wavelengths, x-values, y-values, R squared value, and standard deviation. For each data subset, thousands of wavelengths would be paired.

The last step for the large subsets was to order them on the basis of how many times a given wavelength was repeated in a computation. These “most repeated” wavelengths should therefore be the best and most consistent representation of change in the spectra as the concentration changed because a wavelength would match with more points the better a representation of change it was. These successful relationships could be refined by comparing them to repeated data sets in the lab.

The relationships developed for use in the field had to be replicable and reliable; eliminating relationships that did not repeat in the lab was critical for excluding those that would likely only work under specialized or idealized situations. The first approach was to compare to the previously referenced salt index. The next simplest approach was a correlation analysis, comparing different brine concentrations to a purely salt spectra that also found no trend. The first successful trend, going from tap water to 40 percent brine solution, involved a ratio between

a peak and valley of the brine curve in which the most movement was observed. This successful ratio was then expanded with the aid of Rstudio to check the ratios of all points throughout the curve to each other, regardless of their location on the curve.

3.6 Lab Data Characteristics

First we considered the individual components on their own. Figure 3.9 shows the significant differences of each individual element as detected by the PSR+ hyperspectrometer in the HyLab over the wavelengths 350 nm to 2500 nm.

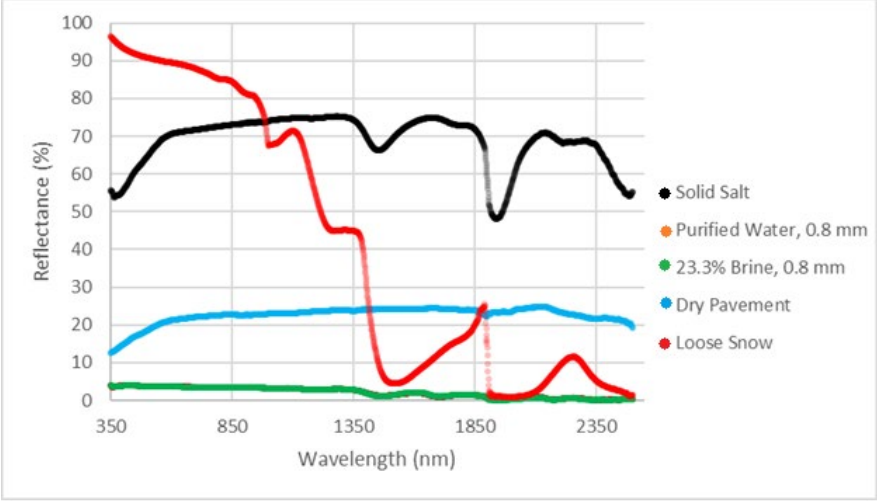

Figure 3.9. Common winter roadway surface materials

Visual inspection indicated that the differences between select prime constituents of a winter roadway were significant, each having their own unique identifiers (i.e., peaks and valleys at specific wavelengths). Solid salt had a very high reflectance over the entire visible spectrum in comparison to asphalt pavement or water. The reflectance properties of water can be so low that, depending on the film thickness, reflectance can reach 0 percent, as shown in figure 3.10. The low reflectance values indicate more absorption of light. Figure 3.10 illustrates the effect of ice film thickness on reflectance.

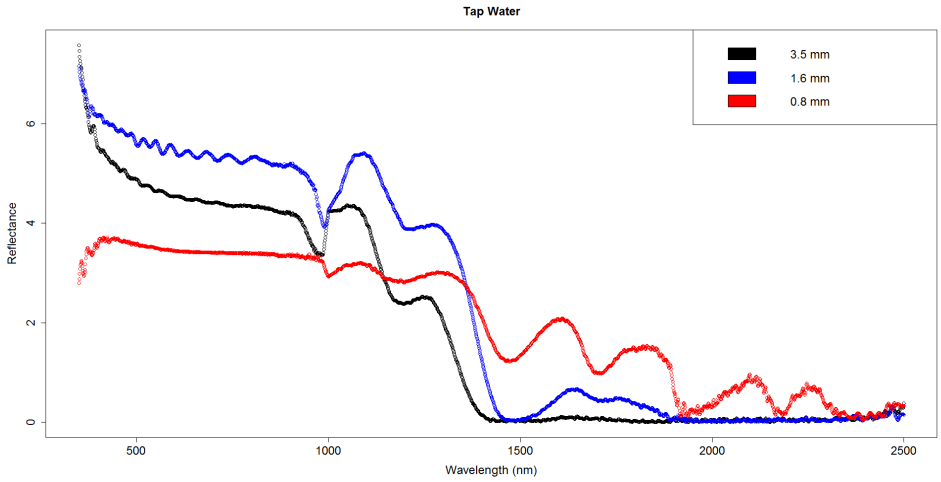

Figure 3.10 Effects on reflectance depending on film thickness

At a film thickness of 3.5 mm, the reflectance took on a value of nearly 0 percent after the 1400-nm wavelength. If a host material or a surface material has a reflectance at or near 0 percent it can make interpretation of other materials present difficult or impossible. Typically, band math overcomes this issue by identifying the effects of certain key absorption points that signify a given material. These key signatures points are manifested on a reflectance curve as a valley. However, a problem discovered while analyzing water films in this research was that materials that have near maximal absorption (e.g., reflectance near or at 0 percent, which absorb all light entering) are not capable of representing the absorptive capabilities of added materials accurately. If a material is already highly absorptive of light with reflectance near 0 percent, then adding more absorption will be negligible and not produce a noticeable change, as shown previously in figure 3.8. A reflectance that is unable to significantly change value because of a very low initial reflectance is problematic because some of the key signifiers for salt absorption lay within the NIR bounds.

The temperature, shape, and imperfections of a target can also have a great impact on the resulting reflectance spectra. For example, the reflectance curves for water vary greatly

depending on its state (liquid, solid, or gas). The impacts of spectra are limited to not only phase changes but may also be influenced by the various physical states that the element may occupy. The grain size of ice and snow, while not necessarily visually significantly different, can produce very different reflectance values depending on crystal size (e.g., fine or coarse snow to solid ice). The effects are shown in figure 3.11 comparing the different types of snow, frost, and ice (ECOSTRESS Spectral Library, 2018).

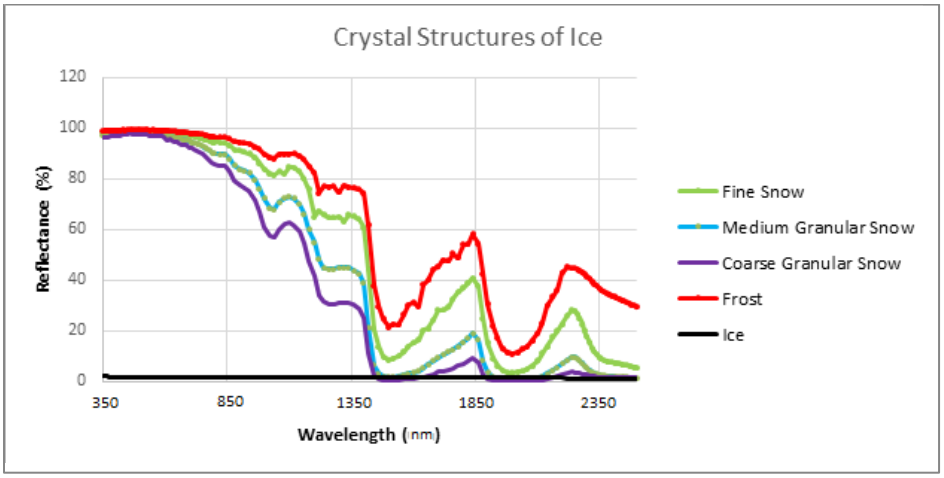

Figure 3.11. Ice crystal differences in reflectance

Since background reflectance can be highly variable because of different coverage percentages (e.g., the ratio of asphalt to ice) and the many differences that variable grain size can cause, this research focused on the changes caused by the addition and manipulation of deicing and anti-icing materials.

Chapter 4. Analysis

4.1. Salt and Brine Comparisons

Analysis for salt began with obtaining ten measurements, which were compared to each other to ensure accuracy and to check for noise and wavelengths that may have had uncertainty in analysis (figure 4.1) before being averaged together for computational analysis (figure 4.2).

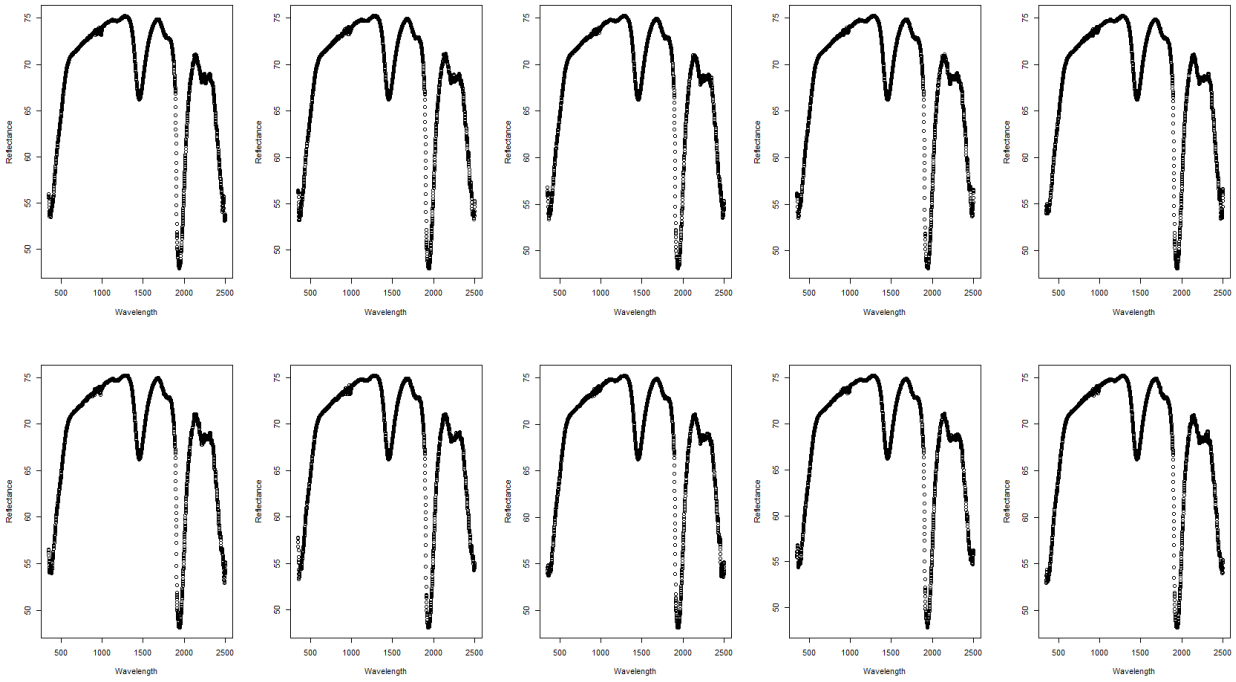

Figure 4.1 Salt crystals: ten measurements in a lab setting (reflectance percentage vs. wavelength nm)

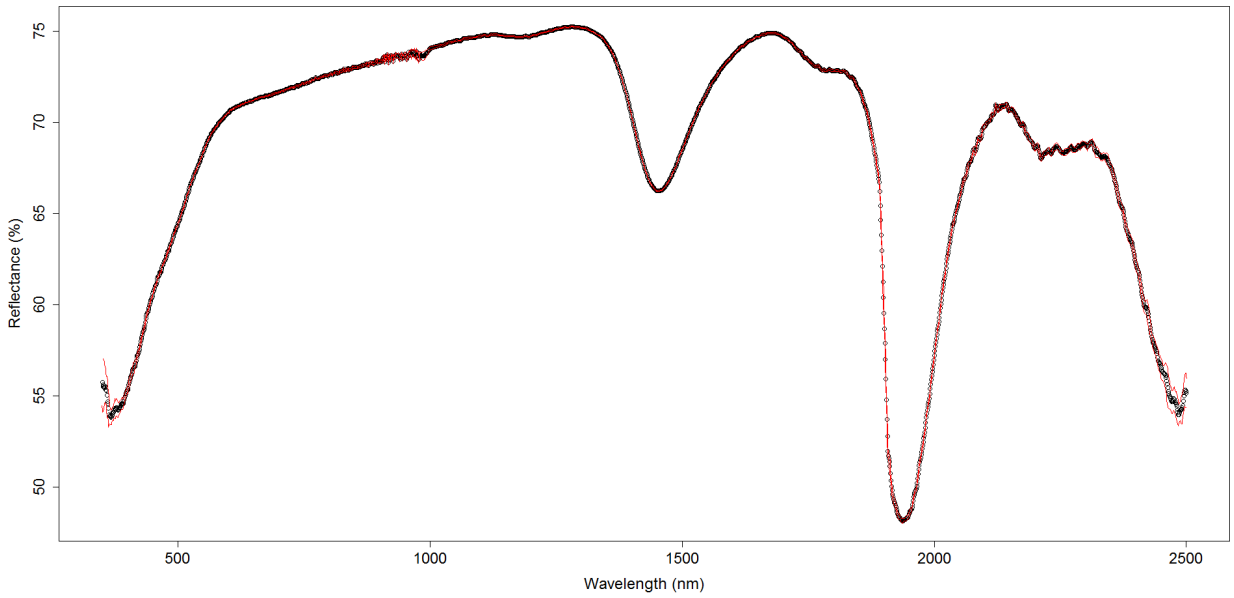

Figure 4.2. Solid salt crystals averaged spectra

These lab-derived measurements of sodium chloride (figure 4.2) were confirmed with existing spectra from a scientific library hosted by ECOSTRESS and shown in figure 4.3. No library currently exists for exact concentrations of brine and beet mixtures, which means that validation with previous studies for these curves would not be possible. Spectra identification for these solutions will be a valuable contribution for anyone pursuing reflectance related work with these materials at different concentrations and thicknesses.

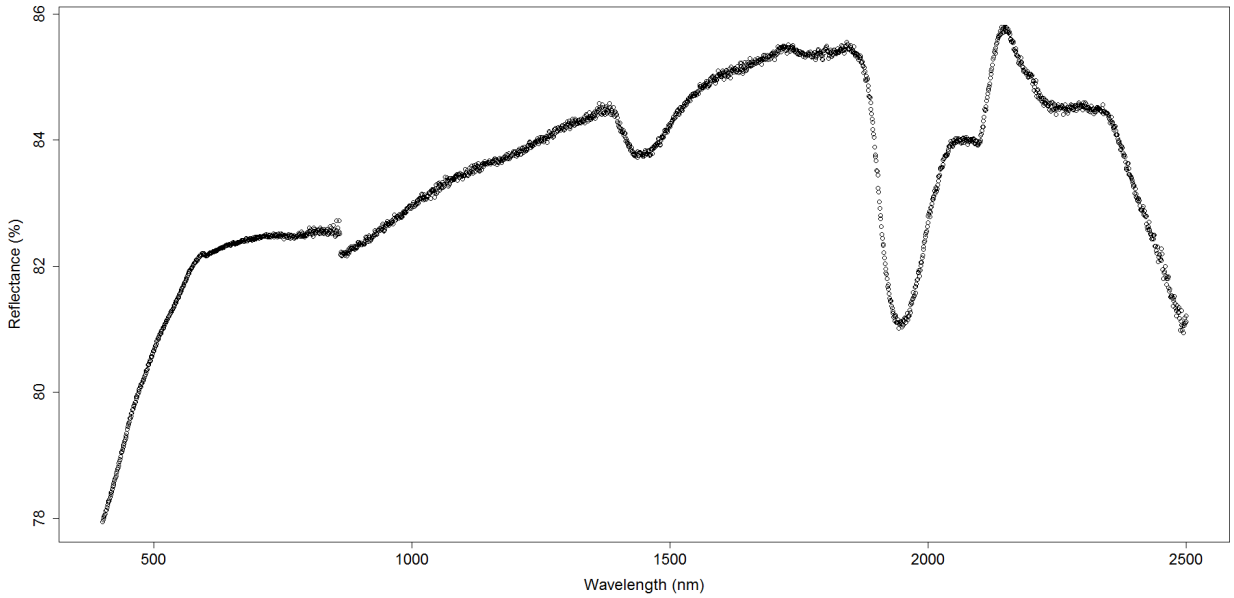

Figure 4.3. Lab salt reflectance

Visual inspection of the curves indicated slight differences around 1450 nm, with the USGS spectral library reporting a much less severe valley and a plateau from 600 nm to 850 nm. These differences are possibly explained by different lighting settings, crystal sizes, surface imperfections, and possibly backgrounds used in this analysis in comparison to those obtained and cataloged in other studies previously. However, both spectra had significant key absorption points (e.g., points where significant absorption caused a dip or valley on the curve). Both the UAF-generated and established online spectra had the same valley locations at about the 1950 and 1450 nm wavelengths. Tthese are key identifiers for salt, as these are the locations of large reflectance changes, confirming the accuracy of the UAF Hylab PSR+ hyperspectrometer.

The solid salt from the AKDOT&PF Northern Region was then dissolved in water to create deicing and anti-icing solutions at three different thicknesses,: 3.6 mm, 1.6 mm, and 0.8 mm. The 3.6-mm height was selected as an upper bound to test the ability to detect salt, as a thicker water layer would have a higher $\frac{mg}{cm^2}$ concentration of salt present. Although a 3.6-mm

film thickness dis not mimic real-world applications of deicing and anti-icing material, it represented an upper bound that could be experienced under conditions of melt and accumulation without proper runoff or a solid salt application on a particularly icy or snowy road. Similarly, a 1.6-mm thickness application was done, and the thinnest application achievable in the lab was 0.8 mm thick, which was still a thicker liquid layer than should be found on a well-maintained road. These different thicknesses could then be used to investigate how much water film thickness would affect the efficacy of hyperspectral readings or derived computations. Each individual concentration and liquid height had 10 different reflectance curves recorded. In other words, each day involved about 60 recordings for this phase of the research. Each curve was then be collated and compared to each other, as demonstrated in figure 4.4.

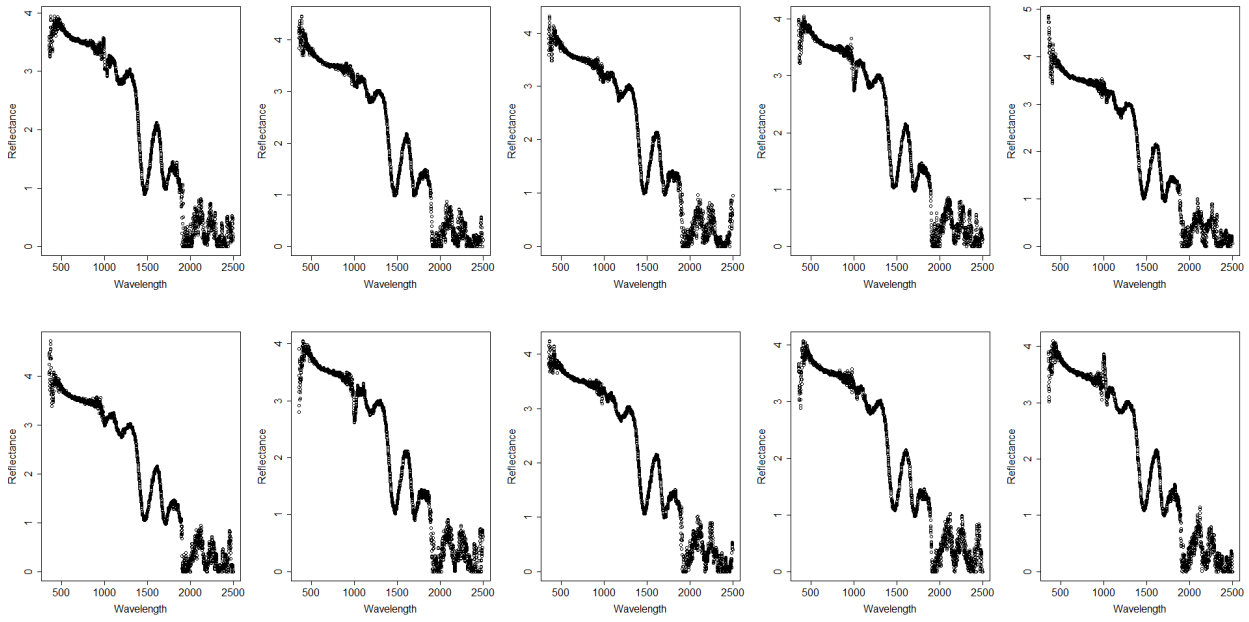

Figure 4.4. Individual 23.3 percent brine reflectances at 0.8 mm, 5mL, Sep 17

The first step, as with all spectra gathered in this research, was to take ten measurements, check for reasonable standard deviation values, and average for computational analysis and comparison.

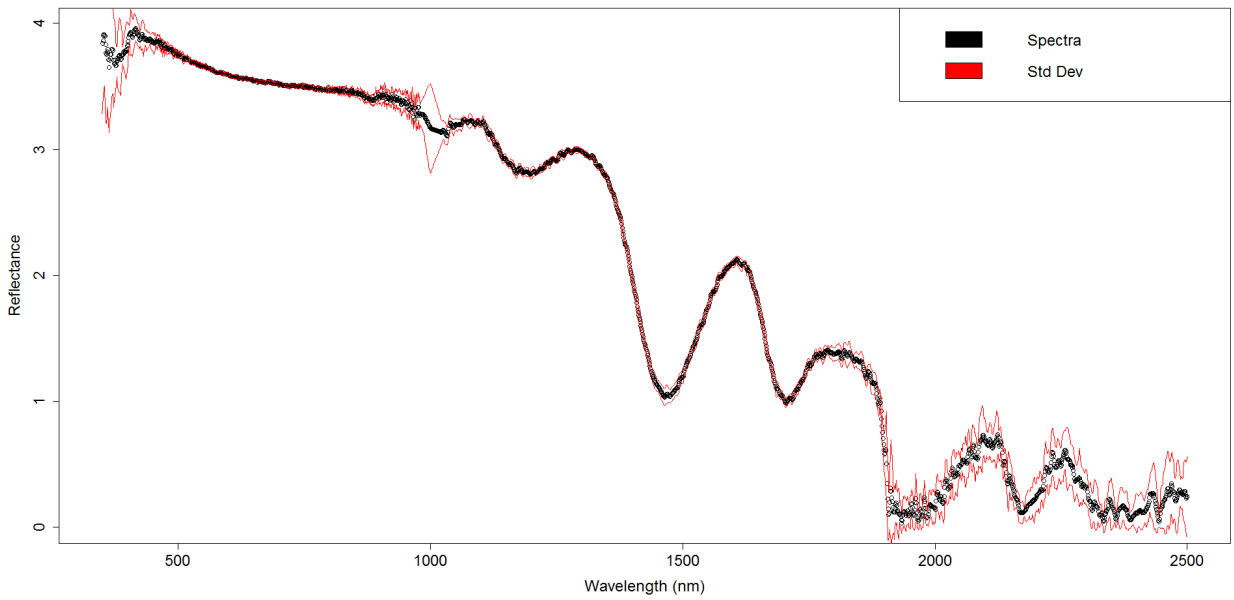

Figure 4.5. Averaged 23.3 percent brine at 0.8 mm, 5mL

The averaged spectral curves were used for comparative and analytic purposes (i.e., to compare a brine of 5 percent concentration to a brine of 10 percent concentration). The red lines in figure 4.5 denote the standard deviation and highlight locations where the derived relationships might need more scrutiny or warrant additional data collection. In general, the deviations from the mean were relatively small, basically zero, with the exception of wavelengths under 475 nm and a small area in the vicinity of the 1000-nm wavelength. This 1000-nm wavelength uncertainty corresponded exactly with a group of uncertainty inherent to the reference panel and in the background material. This uncertainty may have been due to inefficiences of Hylab and lab equipment (i.e., imperfections of the reference panel, wear and tear on equipment, or outdated calibration). Comparing different concentrations and volumes could begin after subsequent spectra were generated.

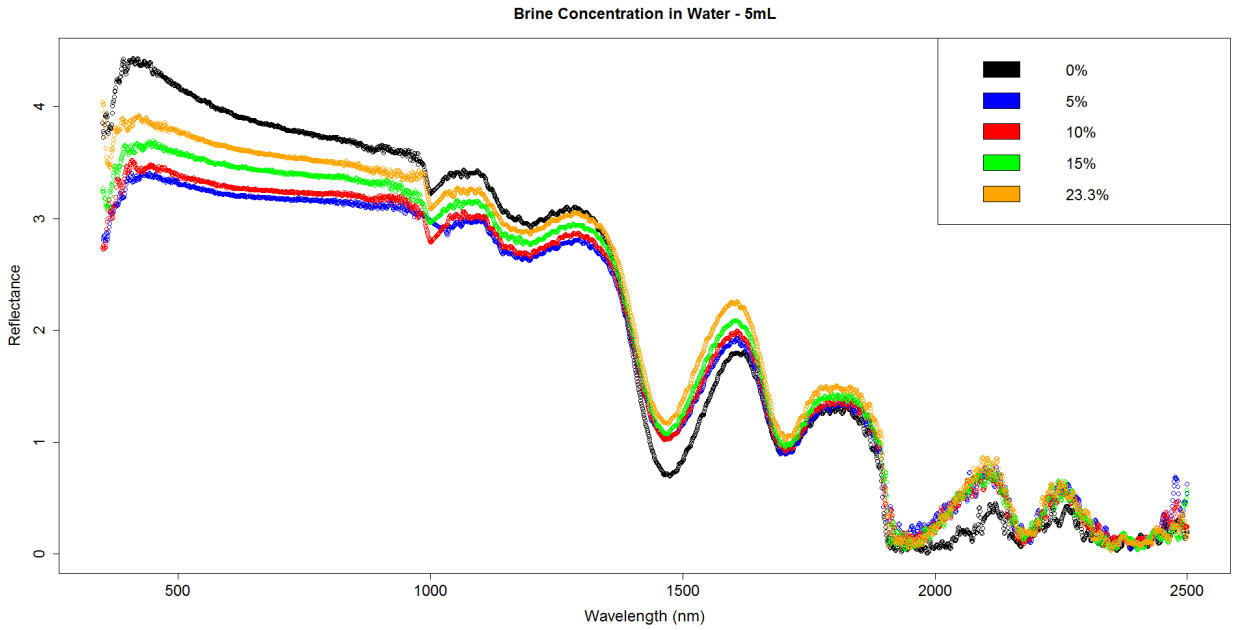

Figure 4.6. Brine concentrations – 5 mL

Visual comparison between the changes in the reflectance spectra as concentration changed was difficult. The changes appeared minor in terms of reflectance, with some added noise beyond the 1800-nm wavelength (see figure 4.6). Mathematical comparisons were then necessary to identify these differences and to obtain relationships to quantify how those changed from one concentration or film thickness to the next (see figure 4.7).

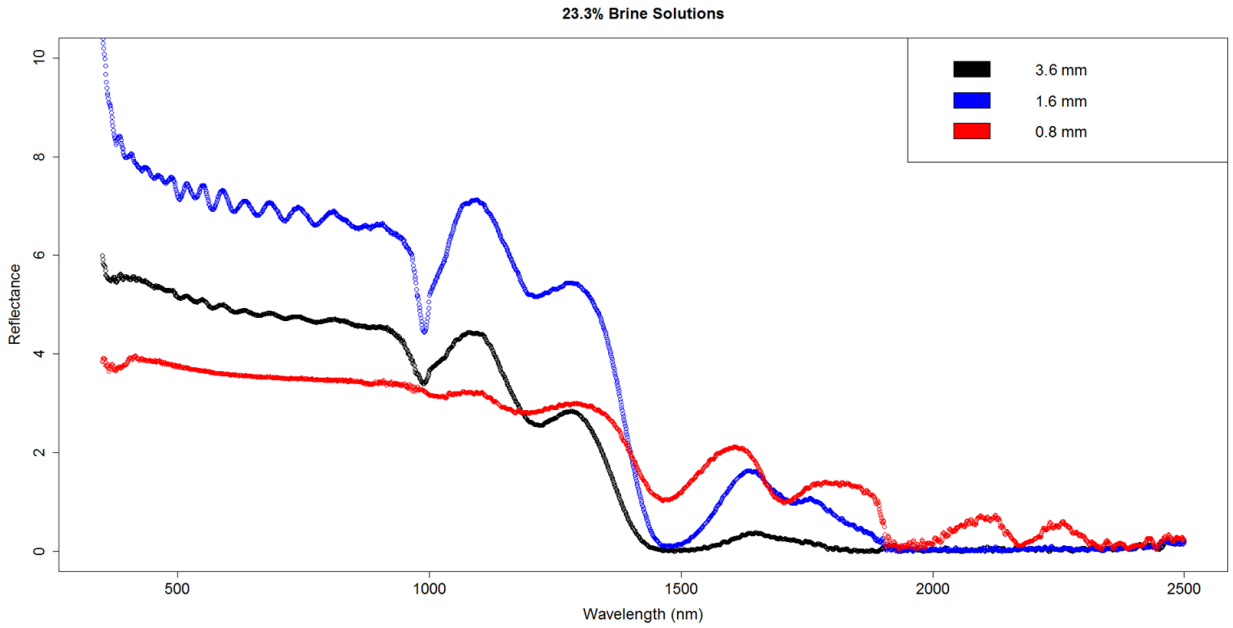

Figure 4.7. Brine film thickness differences

Visually, the differences between film thicknesses were significant (figure 4.7). At less than 1-mm thicknesses, much more of the near infrared spectra was present and usable, with the added benefit of a much smoother curve in the visual spectrum. Peaks, valleys, and natural curvature in the sub-1500-nm wavelength were more pronounced with a thicker film. However, the opposite was true at wavelengths exceeding 1500 nm. Validation by replication of the 0.8-mm brine films indicated perfectly matching trends and curve features, yet slight deviation in magnitude can be seen (figure 4.8).

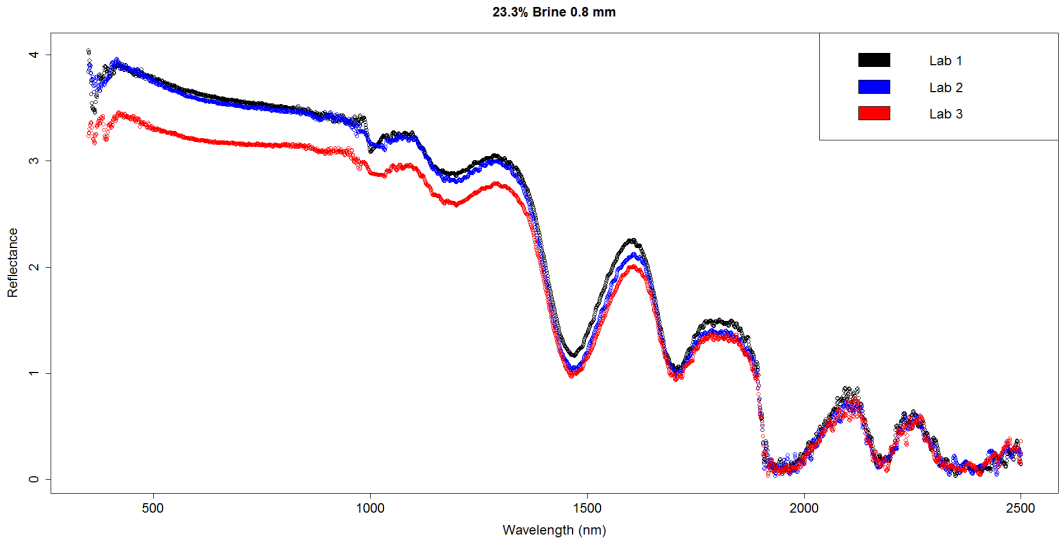

Figure 4.8. Replicated 0.8-mm, 23.3 percent brine

Slight shifts in reflectance values were expected because of the nature of the device and the tendency for there to be small changes in the surrounding environment (reflective surfaces such as metals, ice, or snow). However, the magnitude of these variations was relatively small, and the shape of the spectra was expected to remain nearly the same. Normalizing reflectance to a point such as the 700-nm wavelength revealed the graphs were even more accurate in repetition than shown in figure 4.8, as shown in figure 4.9.

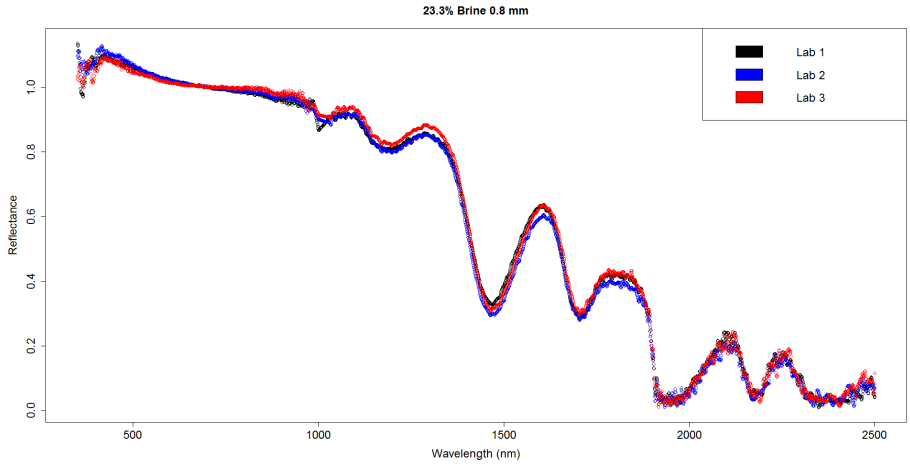

Figure 4.9. Replicated 0.8-mm, 23.3 percent brine normalized to 700 nm

4.2. Beet Comparisons

Beet extract is a visually striking liquid in comparison to the clear brine, as shown below, which suggested that the visual spectrum would be the key absorption points. Analysis for beet juice solutions (Figure 4.10) mimicked the process used for brine solutions.

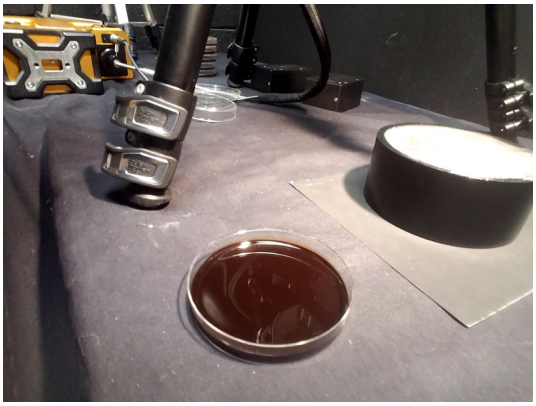

Figure 4.10. Beet solution in a petri dish

Ten samples of the spectra were obtained and then compared to each other to ensure accuracy, identify areas of noise, and determine wavelength uncertainty (Figure 4.11).

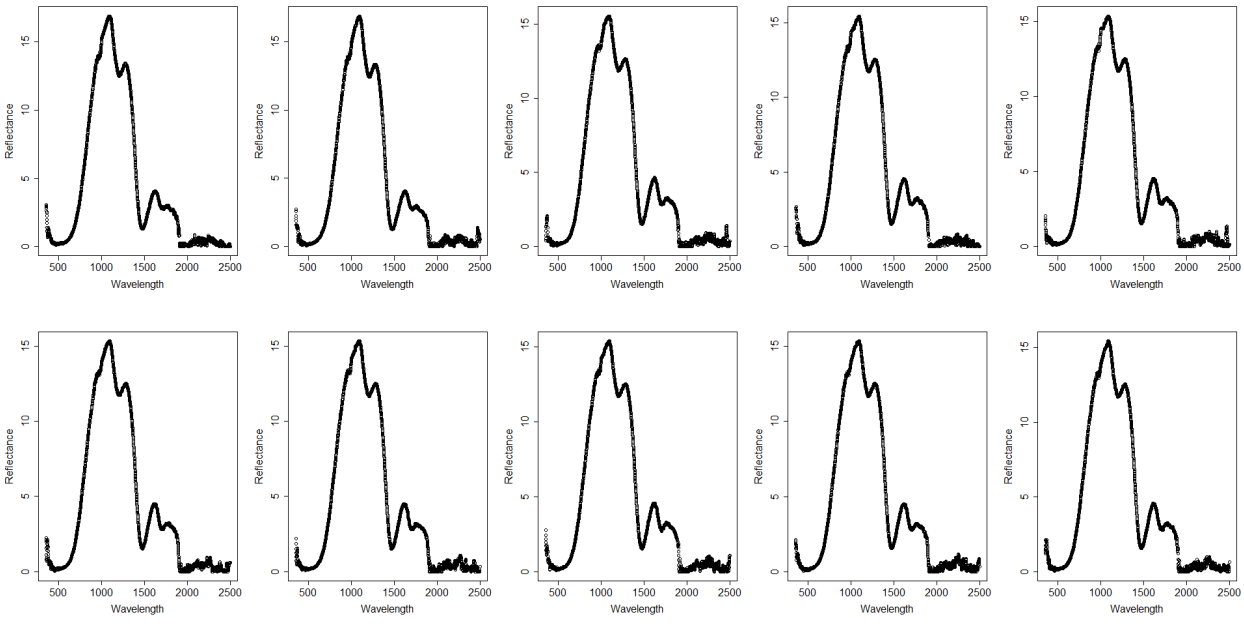

Figure 4.11. 100 percent beet juice initial measurements at 0.8 mm, 5mL, Sep 21

The lab measurements of the beet extract utilized by the AKDOT&PF Northern Region for deicing and anti-icing purposes could not be validated by a comparison with any existing online-hosted libraries. After the reliability of the PSR+3500 unit had been confirmed with the brine analysis, it was a safe assumption that the spectral curves obtained for the beet solutions would be accurate representations. The average of the ten measured spectra and the associated standard deviation are shown in figure 4.12.

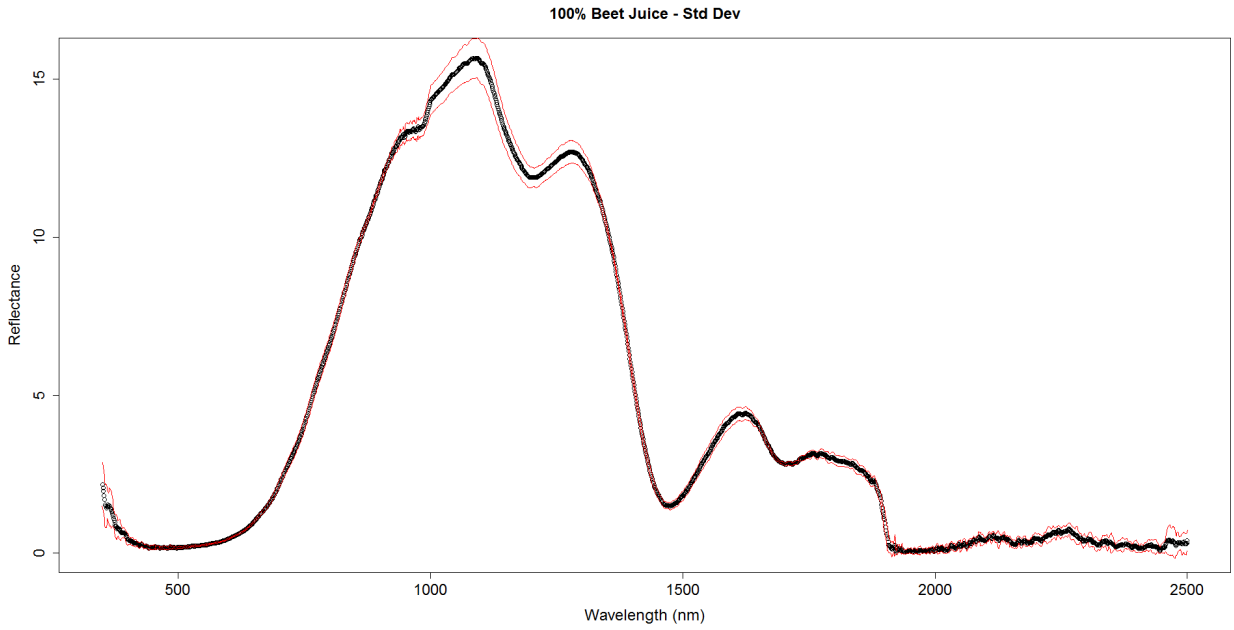

Figure 4.12. Averaged 100 percent beet juice initial measurements at 0.8 mm, 5mL, Sep 21

The maximum concentration of beet extract applied by AKDOT&PF is 20 percent, and it is only used in conjunction with a 23.3 percent brine mixture. A dilution point of 10% beet was also selected for comparison to the full 20 percent beet and the pure 100 percent beet spectra.

An increase in beet juice concentration caused significant changes in the reflectance spectra, as shown below in figure 4.13. Adding beet juice had significant impacts on the visual spectrum and the NIR spectrum. The visual spectrum got absorbed, with higher concentrations of beet juice obliterating the reflectance values over a larger swath of the visual spectrum while

simultaneously increasing the reflectance in the NIR. At 100 percent concentration, the visual spectrum was absorbed nearly completely until the 550-nm wavelength, and the inflated reflectance began to trend toward a reflectance mimicking that of tap water at the 1450-nm wavelength. The changes were much more muted beyond this point, even approaching a near-zero value after the 1900-nm wavelength.

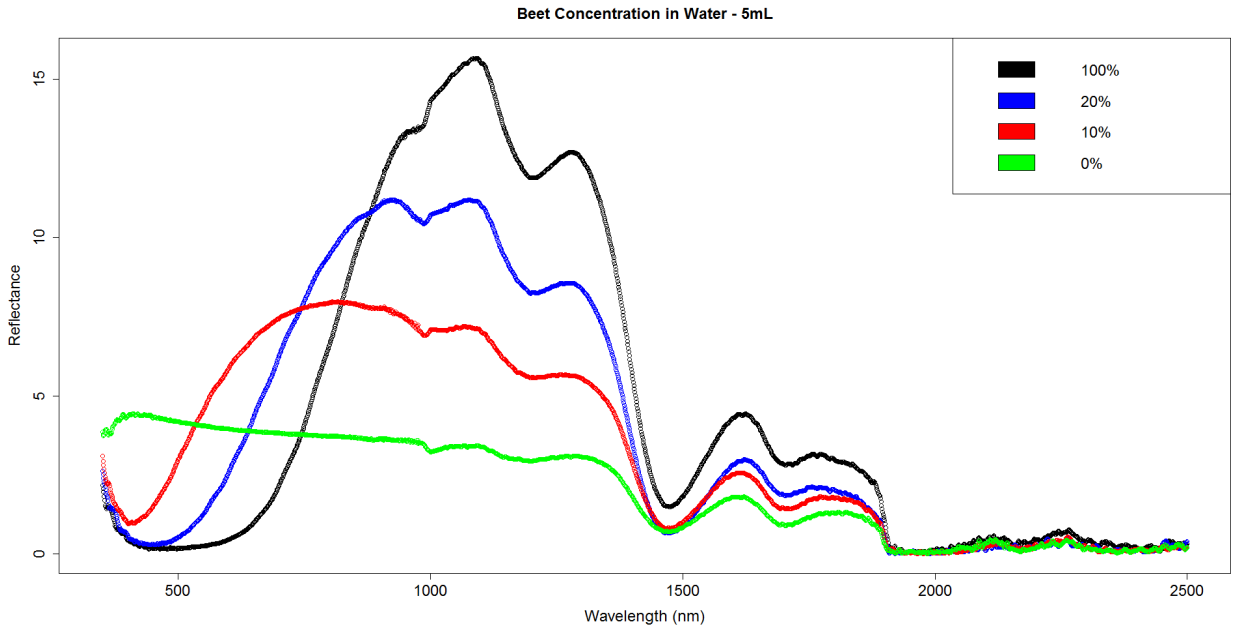

Figure 4.13. Beet juice reflectance differences in concentration

Differences in the reflectance based on liquid volume were significant, much like the brine differences shown previously in figure 4.7. The increasing thickness again obliterated the NIR and IR wavelengths as thickness increased. However, as seen in figure 4.14, the beet differences showed the maximum reflectance at the intermediate point of 1.6-mm thickness.

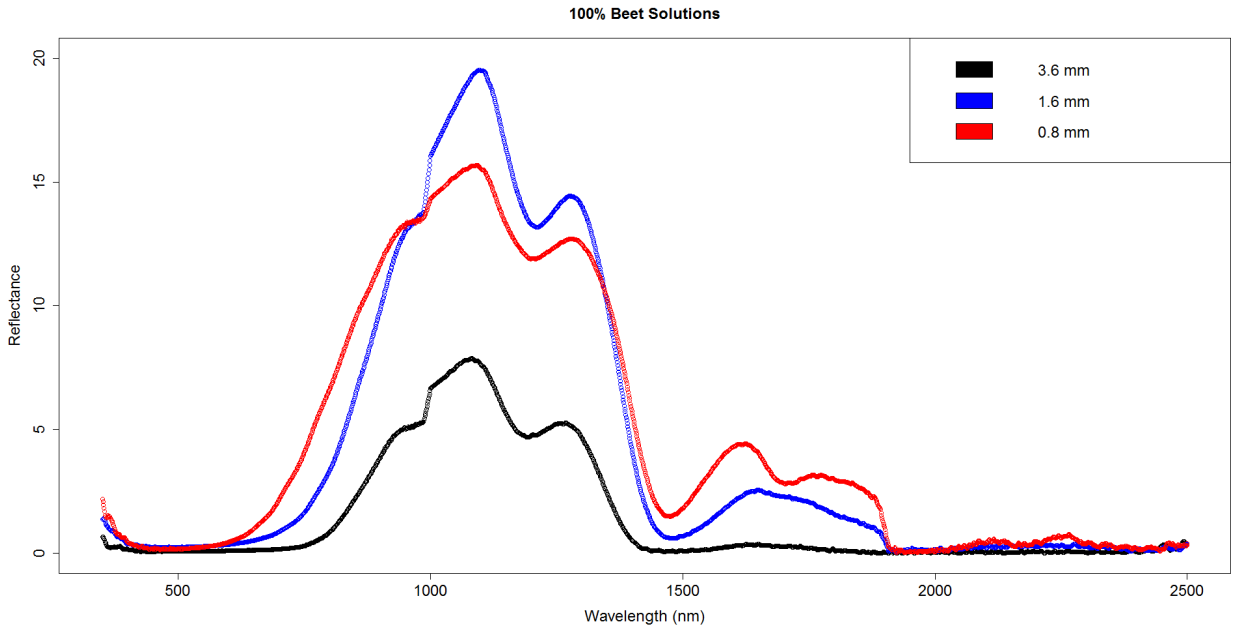

Figure 4.14. 100 percent beet film thickness differences

Repeatability with the beet solutions was less perfect than with the pure brine mixtures, with notable visual differences around the 1000-nm wavelength. However, there was reasonable replication along the entirety of the spectrum, except for wavelengths in the vicinity of 1000 nm (figure 4.15).

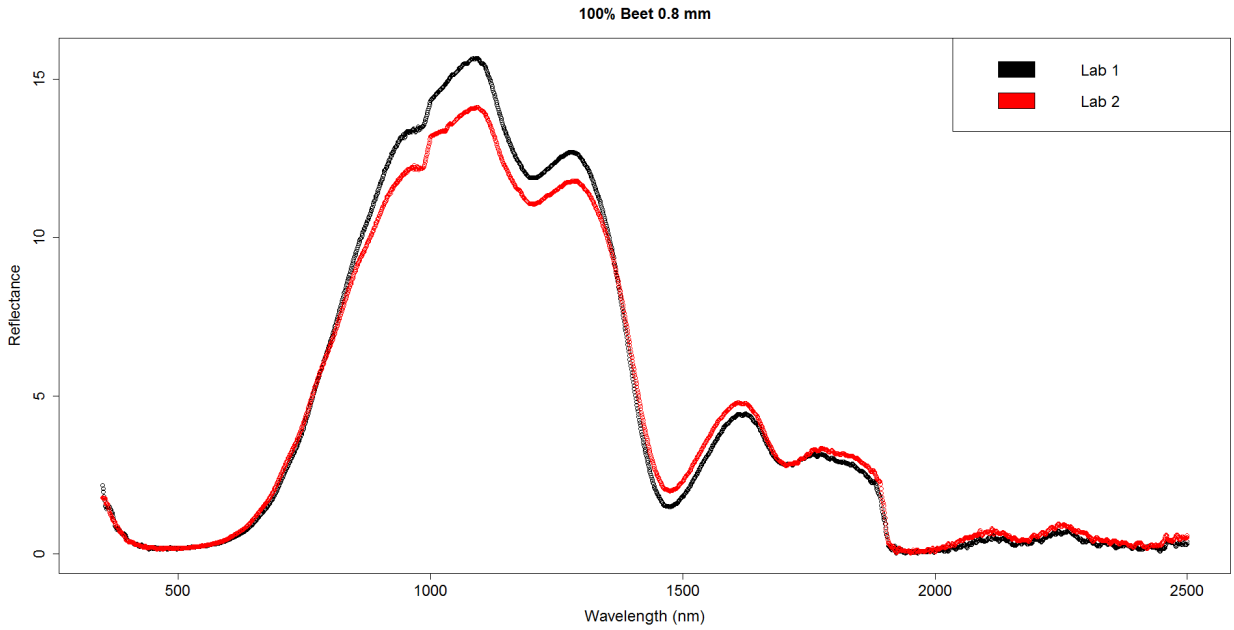

Figure 4.15. Replicated 100 percent beet 0.8 mm

For actual roadway applications in the AKDOT&PF Northern Region, beet extract concentrations will not exceed 20 percent by volume. Comparing these reduced concentrations also reduced the effects of the beet juice, showing a dampening of overall reflectance values and a diminishing of the severity of the peak around the 1000-nm wavelength. The differences between the 0.8-mm thickness and the 1.6-mm thickness were less, as shown in figure 4.16, than the differences demonstrated in the 100 percent beet concentration shown in Figure 4.14.

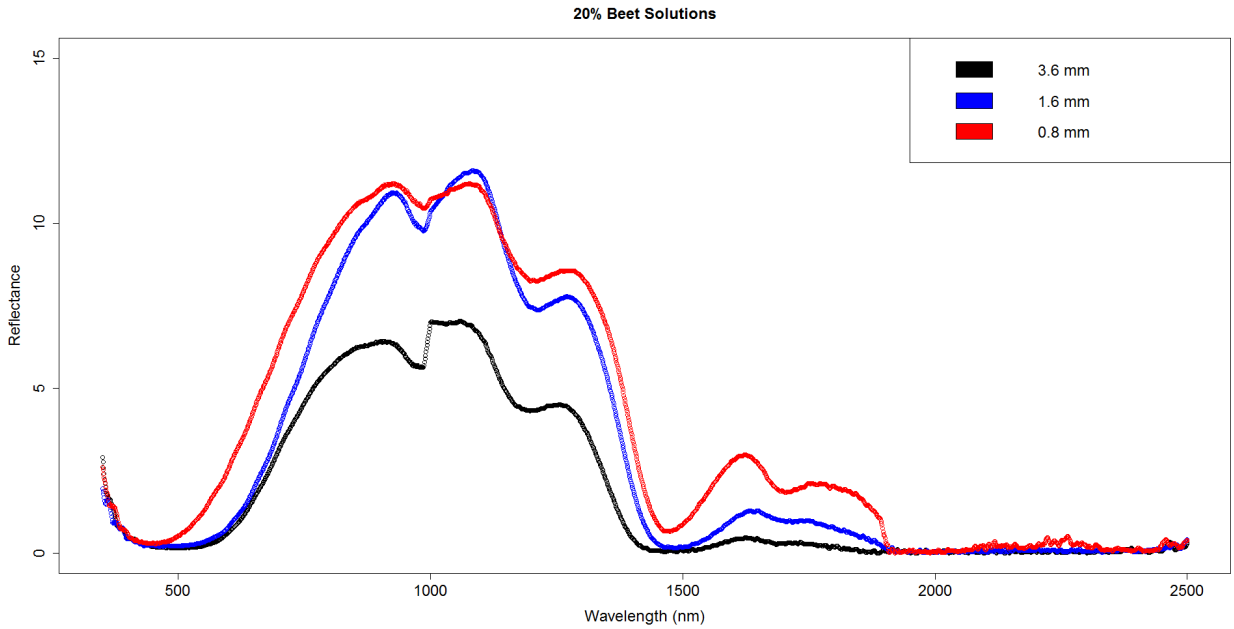

Figure 4.16. 20 percent beet film thickness differences

The replication of 20 percent beet (figure 4.17) shared the same differences as the differences seen in figure 4.15. This repeating artifact suggested the possibility of changes to the chemical over time. This could have been a result of microbial activity feeding off the high sugar content found in beet extract, or some other unrecorded factor.

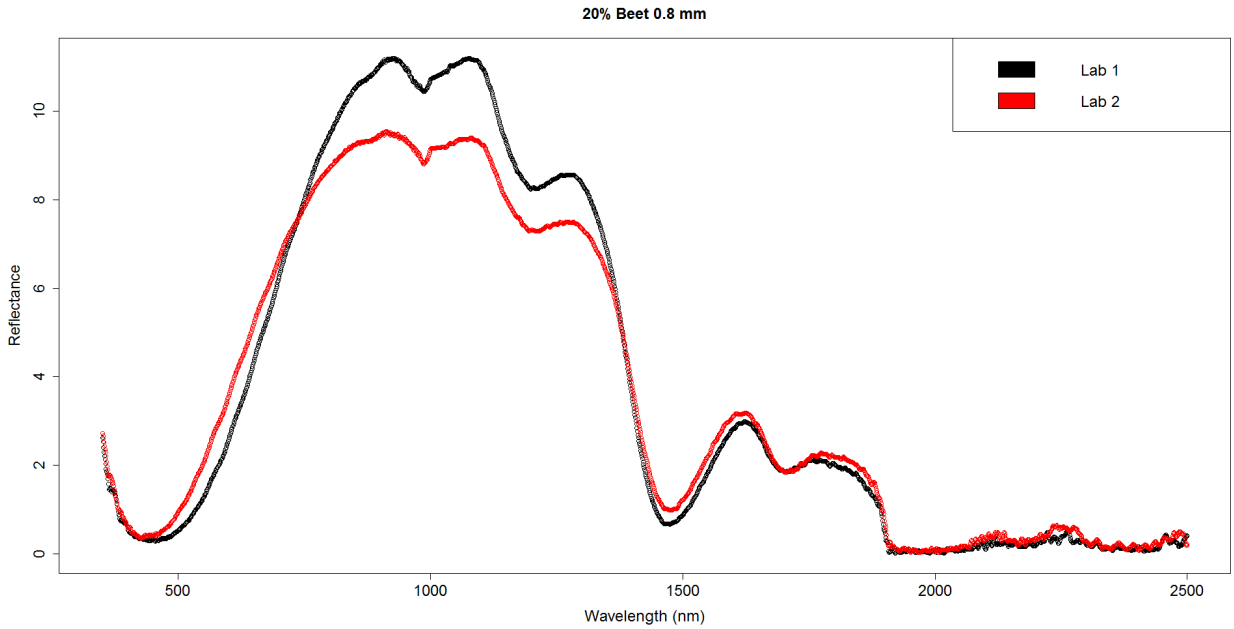

Figure 4.17. Replicated 20 percent beet 0.8 mm

4.3. Beet-Brine Solution Comparisons

Analysis for beet-brine anti-icing and deicing mixture began with taking ten measurements over a short period of time of each sampled concentration. These spectra could be compared to each other to ensure accuracy and then averaged together, as was done in the previous analyses, to identify variations and uncertainty. Figure 4.18 shows the first ten spectra recorded, and figure 4.19 shows the subsequent averaged curve in black and red lines denoting standard deviation.

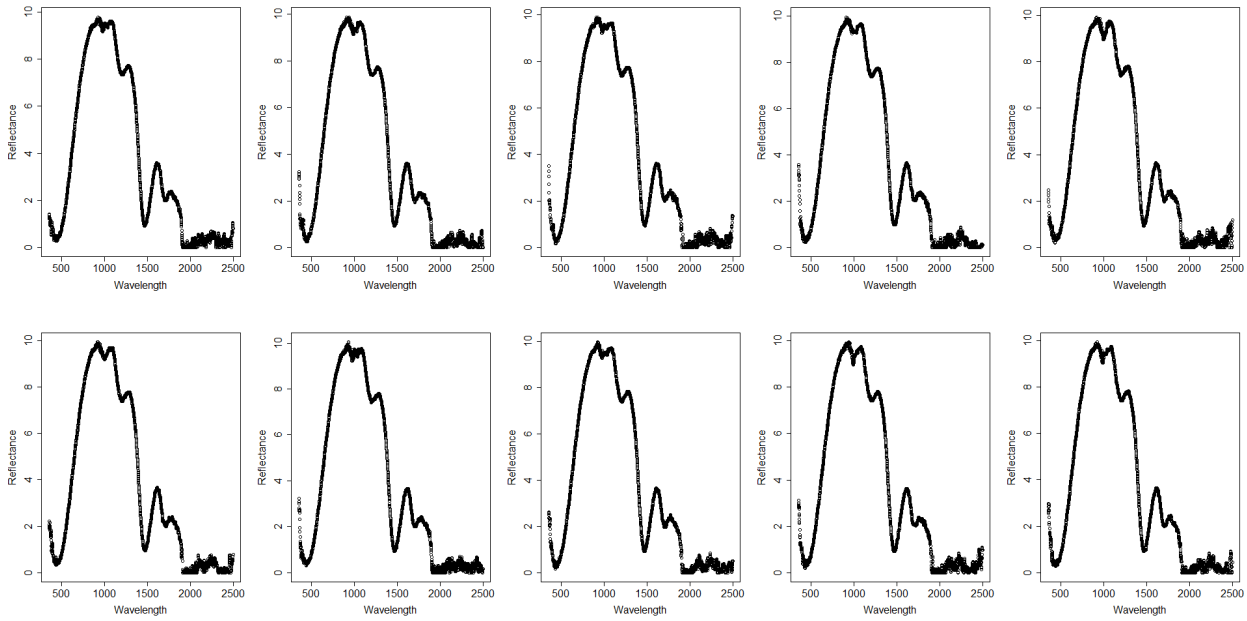

Figure 4.18. 23.3 percent brine 20 percent beet initial measurements at 0.8 mm, 5mL

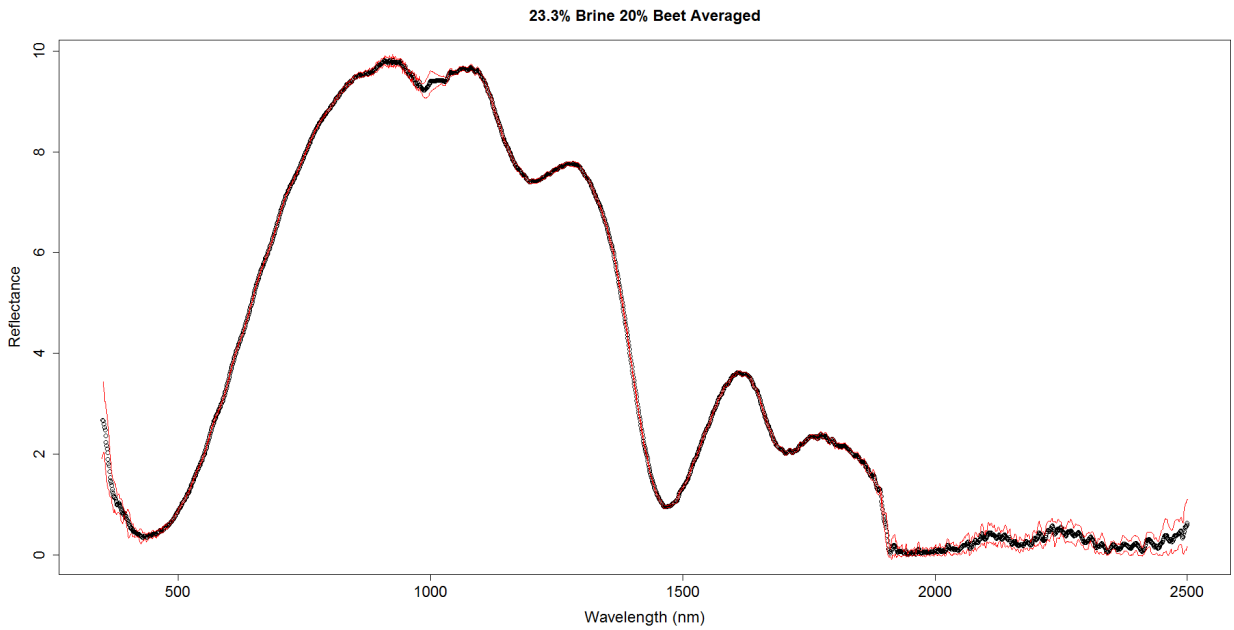

Figure 4.19. Averaged 23.3 percent brine 20 percent beet initial measurements at 0.8 mm, 5mL

The impact of changing solution thickness followed the same trends established by the brine solutions, shown previously, once a wavelength of 1450 nm had been exceeded. These are compared and demonstrated in figure 4.20.

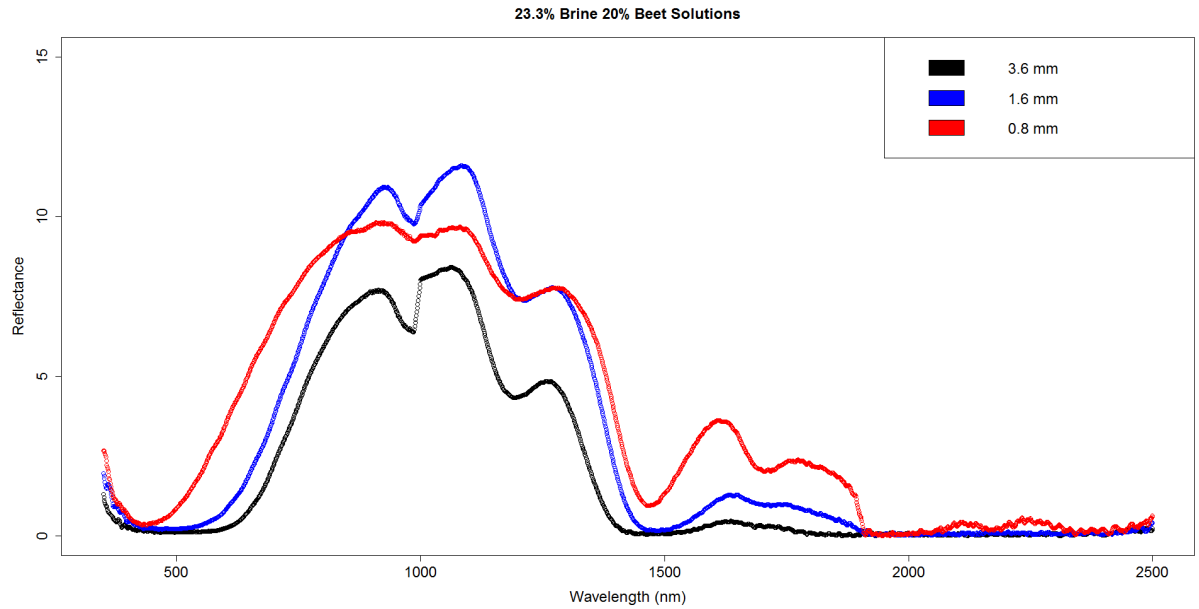

Figure 4.20. 23 percent brine 20 percent beet film thickness differences

Interestingly, the reflectance values did not follow the same trend for brine around the 1000-nm wavelength. Instead, the 1.6-mm thickness had the highest reflectance value. Replication of the 0.8-mm thickness also showed slight changes, as shown in figure 4.21

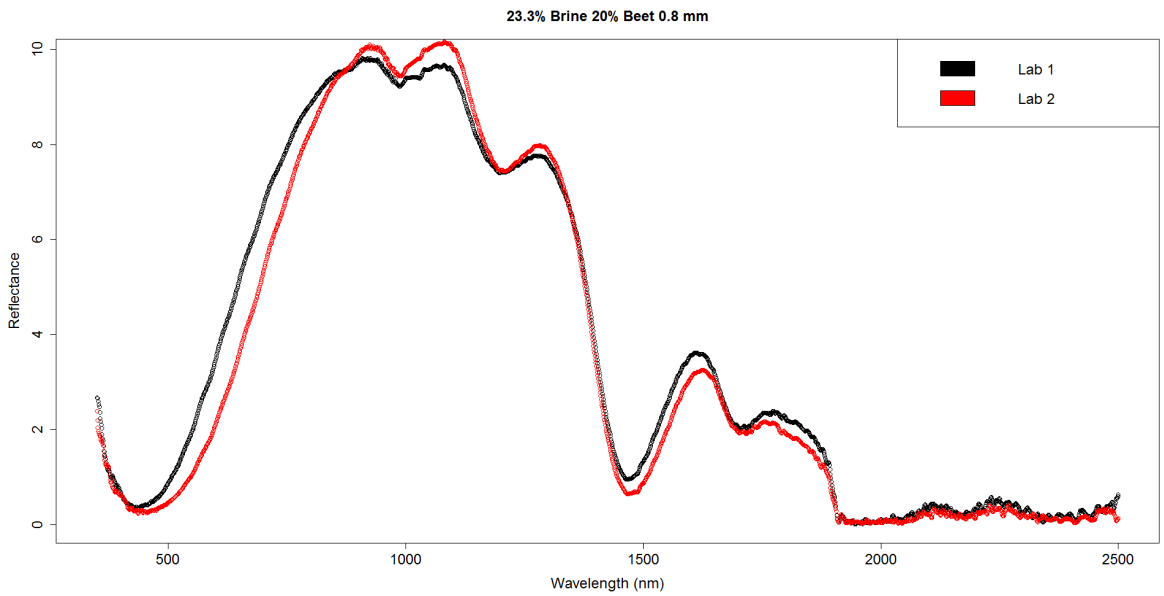

Figure 4.21 Replicated 23.3 percent brine 20 percent beet 0.8 mm

Slight shifts in reflectance values were expected because of the nature of the device and the ability for slight shifts in environment; however the shape of the spectra was expected to remain the same. These slight changes could, again, have been a result of slight microbial activity between the time the samples were obtained from AK DOT&PF and when the spectra were generated.

4.4. Correlation Analysis

Correlation was one of the first attempted metrics used to analyze the spectra gathered from the different brine concentrations. If a clear correlation could be found from the comparison of the solid salt spectra to brine solutions of different concentrations, the correlation factor could be used to identify presence, or possibly even concentration, of the amount of brine present. For correlation analysis, the statistical package R was used. When correlation factors were checked there was not a relationship between increasing sodium chloride concentration in water and correlation to solid sodium chloride. The correlation was checked comparing 1) the complete

spectral curve; 2) a truncated curve that excluded wavelengths past the 1400-nm wavelength where water cuts obliterated the curve; and 3) smaller areas around key identified valleys of the curve. The procedures used for brine were also tested on the pure beet curves without success. Because of ineffectiveness, correlation analysis was abandoned for future use in comparisons.

4.5. Peak and Valley Analysis (Manual)

Peak and valley analysis requires the identification of local minima and maxima of reflectance curves. An example of a range of brine concentrations analyzed is shown in figure 4.22.

Relationship Adjustments

Salt water in petri dish analysis:

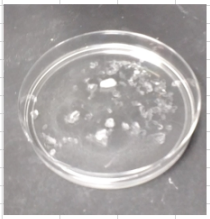

* - logged

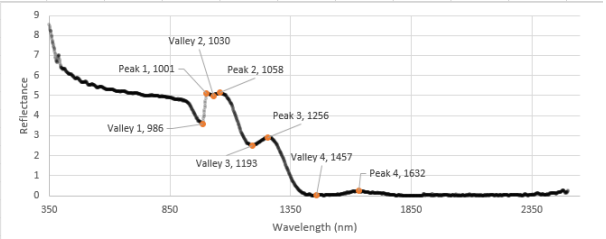

23.3% POI		
feature	x	y
Valley 1	986	3.56587
Peak 1	1001	5.11018
Valley 2	1030	4.98235
Peak 2	1058	5.13705
Valley 3	1193	2.50581
Peak 3	1256	2.91556
Valley 4	1457	0.03988
Peak 4	1632	0.23096

REGULAR	Result						Linear Relationship?			Logged Result*						Logged Linear Relationship?		
Relationship	0	5	10	15	23.3	40	0 to 40	5 to 40	10 to 40	0	5	10	15	23.3	40	0 to 40	5 to 40	10 to 40
V1/P1	0.79328	0.849057	0.78432	0.592232	0.697797	0.763311	0	0	0	0.839543	0.871592	0.838517	0.755799	0.779415	0.885644	0	0	0
V1/P2	0.774537	0.782968	0.759508	0.590003	0.694147	0.752542	0	0	0	0.82586	0.81948	0.820975	0.754473	0.776917	0.880347	0	0	0
V1/P3	1.33666	1.551588	1.360467	1.143071	1.223048	1.135467	0	0	0	1.314895	1.654286	1.322786	1.089888	1.188163	1.064664	0	0	0
V1/P4	31.76435	108.8698	28.38387	21.63712	15.43934	3.348762	0	1	1	-0.53932	-0.31029	-0.60522	-1.1158	-0.86755	2.368504	0	0	0
V1/V2	0.789445	0.808699	0.772493	0.59829	0.7157	0.763263	0	0	0	0.836733	0.839509	0.830133	0.759402	0.79171	0.88562	0	0	0
V1/V3	1.40914	1.696311	1.486179	1.265099	1.423041	1.284032	0	0	0	1.394825	1.907672	1.457896	1.169639	1.384053	1.135744	0	0	0
V1/V4	140.6061	101.8236	169.3367	98.90227	89.41499	5.078972	0	0	1	-0.32447	-0.3162	-0.32593	-0.54539	-0.39462	4.482656	0	0	0
V2/P1	1.004858	1.049905	1.01531	0.989874	0.974985	1.000063	0	0	0	1.003358	1.038217	1.0101	0.995256	0.98447	1.000027	0	0	0
V2/P2	0.981115	0.968182	0.983191	0.986148	0.969885	0.985954	0	0	0	0.987005	0.976142	0.988968	0.993509	0.981315	0.994046	0	0	0
V2/P3	1.693164	1.918623	1.761139	1.910564	1.708883	1.487649	0	0	0	1.571463	1.97054	1.593462	1.435192	1.500756	1.202167	0	0	0
V2/P4	40.23631	134.6235	36.74323	36.16493	21.57235	4.38743	0	1	1	-0.64455	-0.3696	-0.72907	-1.46931	-1.0958	2.674402	0	0	0
V2/V3	1.784976	2.097582	1.923874	2.114525	1.988319	1.682294	0	0	0	1.666989	2.272367	1.756219	1.54021	1.748183	1.282429	0	0	0
V2/V4	178.1076	125.9105	219.2082	165.3082	124.9336	6.654292	0	0	1	-0.38778	-0.37665	-0.39263	-0.71818	-0.49844	5.061602	0	0	0
V3/P1	0.562953	0.500531	0.527743	0.468131	0.490357	0.594464	0	0	0	0.601898	0.456888	0.575156	0.646182	0.563139	0.779791	0	0	0

Figure 4.22 Excel peak and aalley analysis example

An example of the visual inspection identification for the brine curve is shown in figure 4.23, where the valleys and peaks are numbered in order of occurrence from left to right and the point of interest's associated wavelength (nm) is recorded.

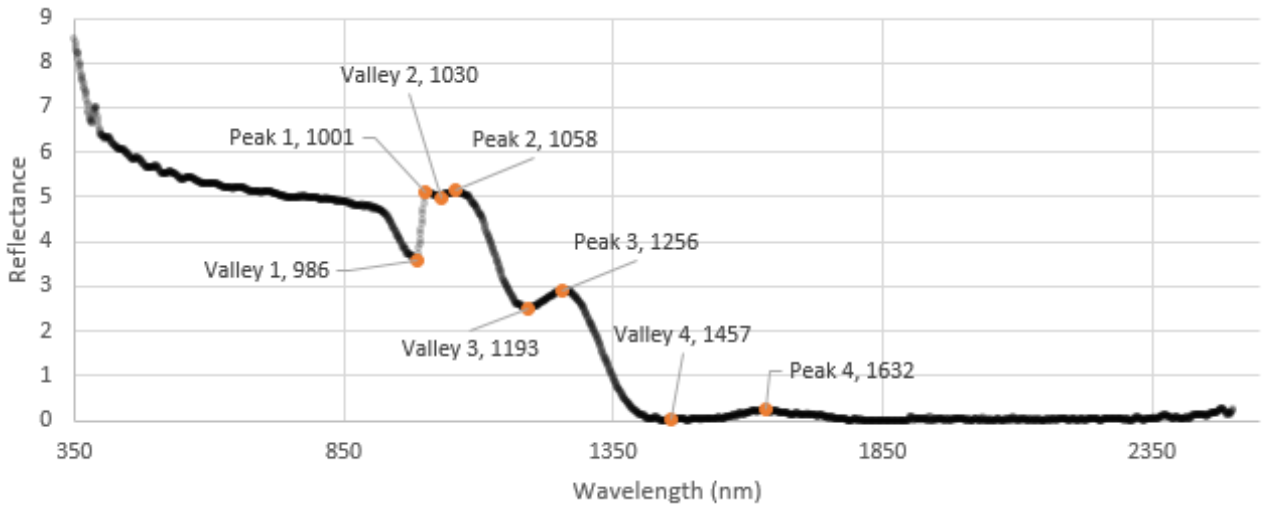

Figure 4.23. 23.3 percent brine at 3.2 mm with key peak and valley points

For the manual peak and valley analysis, the associated wavelengths and reflectance values for each definitive point of interest were extracted from the text files that were generated by the PSR+ spectral imaging unit. These were then loaded into a separate Excel Sheet for additional analysis and comparison. Table 4.1 shows the linear relationship checks from the peaks (P) and valleys (V) extracted from figure 4.23. Analysis started with comparing the trends in these peaks and valleys as concentration changed, comparing them when the reflectance values were offset by 1, and comparing them when they were offset by 1 and normalized, in order to test which permutations would reveal relationships.

Table 4.1. Brine 3.2 mm linear relationship analysis

REGULAR	Result						Linear Relationship?		
Relationship	0	5	10	15	23.3	40	0 to 40	5 to 40	10 to 40
V1/P1	0.79328	0.849057	0.78432	0.592232	0.697797	0.763311	0	0	0
V1/P2	0.774537	0.782968	0.759508	0.590003	0.694147	0.752542	0	0	0
V1/P3	1.33666	1.551588	1.360467	1.143071	1.223048	1.135467	0	0	0
V1/P4	31.76435	108.8698	28.38387	21.63712	15.43934	3.348762	0	1	1
V1/V2	0.789445	0.808699	0.772493	0.59829	0.7157	0.763263	0	0	0
V1/V3	1.40914	1.696311	1.486179	1.265099	1.423041	1.284032	0	0	0
V1/V4	140.6061	101.8236	169.3367	98.90227	89.41499	5.078972	0	0	1
V2/P1	1.004858	1.049905	1.01531	0.989874	0.974985	1.000063	0	0	0
V2/P2	0.981115	0.968182	0.983191	0.986148	0.969885	0.985954	0	0	0
V2/P3	1.693164	1.918623	1.761139	1.910564	1.708883	1.487649	0	0	0
V2/P4	40.23631	134.6235	36.74323	36.16493	21.57235	4.38743	0	1	1
V2/V3	1.784976	2.097582	1.923874	2.114525	1.988319	1.682294	0	0	0
V2/V4	178.1076	125.9105	219.2082	165.3082	124.9336	6.654292	0	0	1
V3/P1	0.562953	0.500531	0.527743	0.468131	0.490357	0.594464	0	0	0

These relationships were tested for linearity including all points, excluding tap water as a relationship point, and excluding tap water and 5 percent brine. Examples of the linear relationship comparisons are shown in figure 4.24.

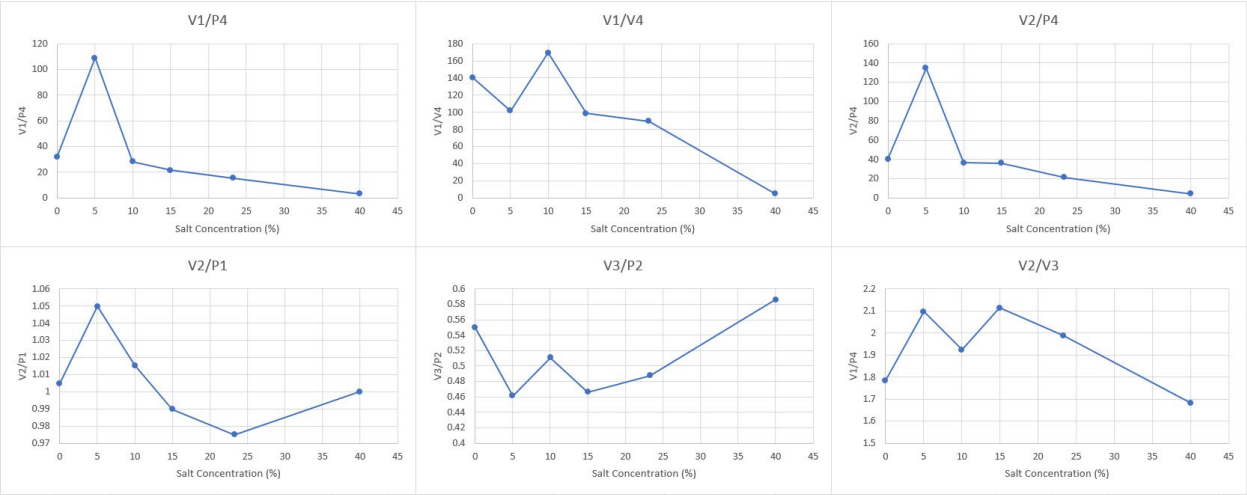

Figure 4.24. Peak and valley ratio linear relationships for salt brine concentrations

The developed linear relationships between peaks and valleys did not generate a relationship that satisfied all "points." The generated relationships, at most, showed a linear relationship using a 10 percent to 40 percent concentration, with the 5 percent and tap water throwing off the curve. In order to generate successful relationships, some possible inadequacies

had to be addressed. First, reflectance values near 0 were problematic because shifts in the curve at or near 0 can resulted in exponential changes in value. Values near zero were addressed by offsetting the curve by a value of 1 to avoid dividing by numbers at or near zero. Second, some vertical reflectance shifts were generated from uncontrolled changes in material and environment. Normalizing the reflectance served to control for these reflectance shifts that were not associated with adjusting brine concentrations. Offsetting and normalizing the curves generated some of the first relationships that showed a linear trend with increasing or decreasing salt concentration and changes in the reflectance values of a curve, as shown in figure 4.25.

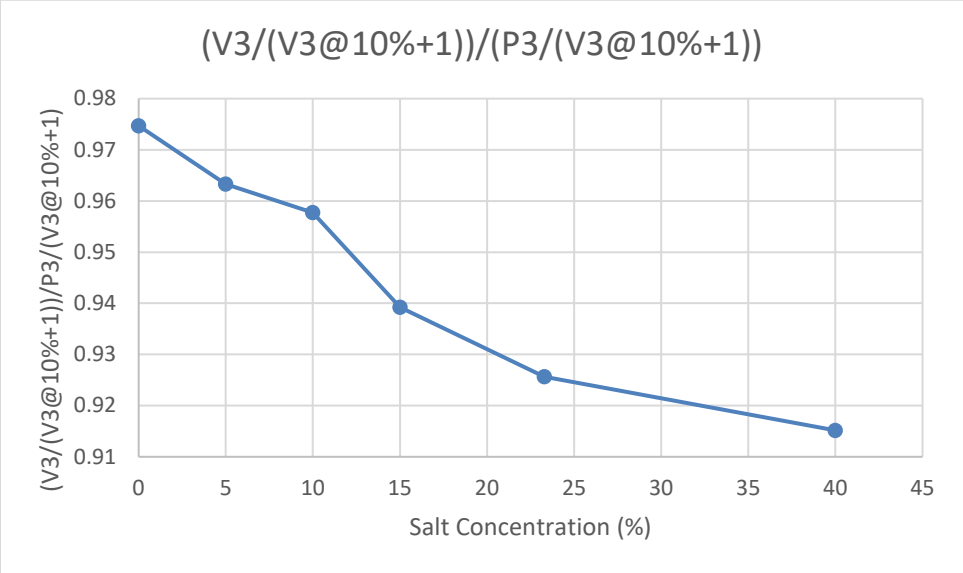

Figure 4.25. Example of successful linear relationship

For the relationship shown in figure 4.25 the band math equation was (B1193/B1193@10% +1)/(B1256/B1193@10%+ 1), where B1256 is the third peak located at wavelength 1256 nm and B1193 is the third valley located at wavelength 1193 nm. The values were then normalized to the third valley of a 10 percent saline solution that was offset by 1. This produced a linear relationship between salt concentration and reflectance recorded in the lab and shows promise for this method, at least in a laboratory setting.

While working relationships were derived from local minima and maxima of the brine, beet, and beet-brine solution spectra, these are not necessarily the best or most consistent relationships for identifying concentration or presence of material. The valleys and peaks in a combined spectrum do not necessarily denote the peak and valleys of an added substance such as the addition of salt to water. Because of this fact and the few relationships gathered from testing just the peaks and valleys, a more rigorous testing method for all possible sources of spectra changes from modification of materials present needed to be developed.

4.6. Peak and Valley Analysis (Automated)

In order to test all possible permutations of wavelength combinations and account for the larger changes occurring away from the peaks and valleys (see previous discussion on the effect of depressions), the statistical package R was used. RStudio code could analyze every single point from the 350-nm wavelength to the 2500-nm wavelength to find relationships as concentrations and film thickness increased or decreased. Figure 4.26 shows an example of the code derived for this purpose. The code starts by selecting a point *j* and comparing it to the same point *I*; then the code iterates *i*+1 until *i* reaches the final wavelength available. The point *j* then iterates by 1 and repeats the process until all point combinations are exhausted.

```
#in the loops i and j had 349 added to them to change it from channel # to wavelength #
for (j in seq(from=1, to=2151, by=1)){
  message(j+349)
  for(i in seq(from=1, to=2151,by=1)){

    if ( ((entity1[i,2]))/((entity1[j,2])) > ((entity2[i,2]))/((entity2[j,2]))
        &((entity2[i,2]))/((entity2[j,2])) > ((entity3[i,2]))/((entity3[j,2]))
        &((entity3[i,2]))/((entity3[j,2])) > ((entity4[i,2]))/((entity4[j,2]))
        &((entity4[i,2]))/((entity4[j,2])) > ((entity5[i,2]))/((entity5[j,2]))
    )
    {
      xvalues=c(xentity1,xentity2,xentity3,xentity4,xentity5)
      yvalues=c(((entity1[i,2]))/((entity1[j,2])),((entity2[i,2]))/((entity2[j,2])),((enti
      lm=lm(yvalues~xvalues)
      entity=(cbind(i+349,j+349,summary(lm)$coefficients[2,1],summary(lm)$r.squared,summar
      entitysuccess=rbind(entitysuccess,entity)
    }


    if ( ((entity1[i,2]))/((entity1[j,2])) < ((entity2[i,2]))/((entity2[j,2]))
      &((entity2[i,2]))/((entity2[j,2])) < ((entity3[i,2]))/((entity3[j,2]))
```

Figure 4.26. Example of RStudio code for iterative linear relationship checking

The resulting tables (see table 4.2) were then analyzed on the basis of which outcome was being tested (e.g., cut-offs for slope, regression coefficient, margin of error, and number of times a given wavelength was found in a data set).

Table 4.2. Example of beginning paired wavelengths from 0.8-mm brine

Sep6 5 mL Lab	Wvl1	Wvl2	slope	R2	Sigma
1	2347	352	-0.00051	0.699229	0.003458
2	354	353	-0.00088	0.981875	0.001244
3	2303	353	0.001727	0.521017	0.017231
4	353	354	0.000895	0.981824	0.001266
5	2303	354	0.001809	0.546578	0.017138
6	2304	354	0.001699	0.552789	0.015894
7	2347	355	-0.00047	0.653186	0.003568
8	2297	357	0.00236	0.485806	0.025257
9	2155	358	0.002369	0.80095	0.012288
10	2156	358	0.002387	0.756787	0.014075
11	2297	358	0.002477	0.553549	0.023144
12	2395	358	0.000259	0.887472	0.000958
13	2154	359	0.002192	0.748242	0.01323
14	2155	359	0.002408	0.828588	0.011395
15	2156	359	0.002424	0.790307	0.01299
16	2395	359	0.000268	0.910297	0.000874
17	2155	360	0.002404	0.82306	0.011595
18	2156	360	0.002421	0.79145	0.012927
19	2296	360	0.002175	0.52231	0.021641
20	2155	361	0.002461	0.846946	0.010883

Comparisons of matching points for the 22-mL application (equivalently a 3.6-mm film thickness) are shown in table 4.3.

Table 4.3. 3.6-mm highest frequency wavelength (nm) for (a) Test 1 (June 15th), (b) Test 2 (January 24th), and (c) the resulting matched values

15-Jun	22 mL
Wvl (nm)	Freq
1923	1137
2036	1101
2058	1098
2120	1074
2037	1057
2161	1056
2162	1032
2160	938
2119	924
2035	884
2118	873
2445	632
1024	539
1023	538
1025	537
1026	534
1028	532
1029	532
1027	531
1030	530

(a)

+

24-Jan	22 mL
Wvl (nm)	Freq
1861	1374
2146	1347
1860	1326
2145	1283
2335	1223
2334	1182
2120	1124
1897	1060
2057	955
2333	931
1938	813
1544	752
1909	702
1898	687
1937	673
1859	653
2447	629
2446	596
2495	555
2210	528

(b)

=

Repeated	22 mL
Wvl (nm)	Freq
2120	871
2446	279
2118	173
2445	161
2119	122
1282	50
1283	48
1281	47
1280	46
1284	45
1273	43
1279	42
1272	41
1278	41
1285	41
1277	40
1286	40
1274	39
1275	39
1276	39

(c)

In analyzing the 22-mL solutions from table 4.3a (June) and table 4.3b (January), the most common points to have relationships with increasing or decreasing salt concentration were found in the NIR wavelengths (approximately 2000 nm and greater), which dominated the top 20 repeated wavelengths. Wavelengths in the NIR spectrum were surprising, given how close to 0 the reflectance values for the brine spectra were beyond the 140- nm wavelength. Repeated values were checked by sequentially testing wavelengths, which resulted in frequently occurring paired values, including several in the region of 2120 nm and 2446 nm. Strong relationships were also observed in the 1275-nm region. These points would have to be checked against points

discovered in the 1.6-mm and 0.8-mm heights to determine whether indeed this relationship for brine worked for all film thicknesses or just the 3.6 mm.

Similarly, table 4.4 shows the results from the thinner, 10-mL liquid application, which was equivalent to a 1.6-mm thickness.

Table 4.4. 1.6-mm highest frequency wavelength (nm) for (a) Test 1 (June 27th), (b) Test 2 (July 9th), and (c) the resulting matched values

27-Jun	10 mL
Wvl (nm)	Freq
2083	1677
2084	1656
2041	1593
2363	1571
2145	1521
1995	1514
2364	1459
2035	1374
2287	1374
2163	1230
1484	1160
1534	1133
1533	1124
1668	1116
1892	1116
2342	1109
1667	1105
1891	1102

(a)

+

9-Jul	10 mL
Wvl (nm)	Freq
1535	1426
1534	1422
1533	1404
1536	1393
1588	1389
1559	1383
1393	1381
1589	1380
1558	1379
1560	1379
1587	1379
1392	1374
1394	1374
1391	1371
1402	1371
1538	1371
1561	1371
1390	1370

(b)

=

Repeated	10 mL
Wvl (nm)	Freq
1484	1073
1534	1070
1668	1064
1533	1063
1667	1051
1680	1045
1679	1038
1678	1036
1669	1030
1483	1029
1677	1007
1507	1001
1508	997
1482	993
1666	975
1532	973
1500	953
1535	944

(c)

Comparing the successful relationships from the first lab group of 5 mL (a) to the second (b) and third group (c) of 5 mL showed that the derived relationships were not consistent. Many relationships that were derived in the first lab iteration did not show up in the second or third lab testing (see table 4.5).

Table 4.3. 0.8-mm highest frequency wavelength (nm) for (a) Test 1 (September 6th), (b) Test 2 (September 17th), and (c) Test 3 (January 28th)

6-Sep	5 mL
Wvl (nm)	Freq
2466	1541
2155	1410
2154	1349
2156	1336
1897	1322
1539	1280
1540	1270
1538	1201

(a)

17-Sep	5 mL
Wvl (nm)	Freq
1912	1797
1913	1788
1911	1595
2426	1482
2425	1480
2427	1394
2428	1091
2355	1026

(b)

28-Jan	5 mL
Wvl (nm)	Freq
1935	1743
1930	1596
2159	1581
2495	1356
2009	1273
2010	1193
2235	998
2237	998

(c)

A more consistent array of wavelengths was achieved by matching the linear relationships between concentration and reflectance ratios. If the matching points from each data set were extracted, nearly 90 percent of wavelength relationships were eliminated, as shown in the first extraction (a) and second extraction (b) in table 4.6.

Table 4.6. 0.8-mm highest frequency wavelength duplicates (nm) for (a) the resulting matched values (Jan 28th and Sep 17th) and (b) the resulting matched values (Jan 28th, Sep 17th and Sep 6th)

Extracted Once	5 mL
Wvl (nm)	Freq
1930	273
507	154
1407	137
1406	135
1408	132
1409	122
1405	119
1398	115
1400	112
1397	111
1399	111
1410	109
506	108
1401	108
1396	103
1402	100

(a)

Extracted Twice	5 mL
Wvl (nm)	Freq
1407	111
1408	109
1406	107
1409	101
1398	95
1410	95
507	94
1397	93
1405	92
1399	89
1400	88
1411	86
1396	85
1401	84
1402	79
1412	79

(b)

The extraction of points made a significant difference in the array of wavelengths shown to have the highest successful relationship frequency. The third extraction also showed that there were sharp diminishing returns for impacts produced by repeated duplicate comparisons. The top 20 frequencies for 0.8-mm brine liquid showed an overwhelming impact by wavelength region from 1395 nm to 1415 nm.

Of the three highest frequency wavelengths identified (first three rows of table 4.6), the top three (1407, 1408, and 1406) repeated at a frequency of 111, 109, and 107, respectively. In total, 97 wavelengths were shared between the three groups. These repeated values were likely to hold constant when salt concentration changed. Conversely, the points 1407, 1408, and 1406 experienced the greatest changes in the curve once normalized to themselves. The wavelengths

were drawn (vertically) on a curve of 23.3 percent brine 0.8-mm thick liquid film spectral curve shown in figure 4.27.

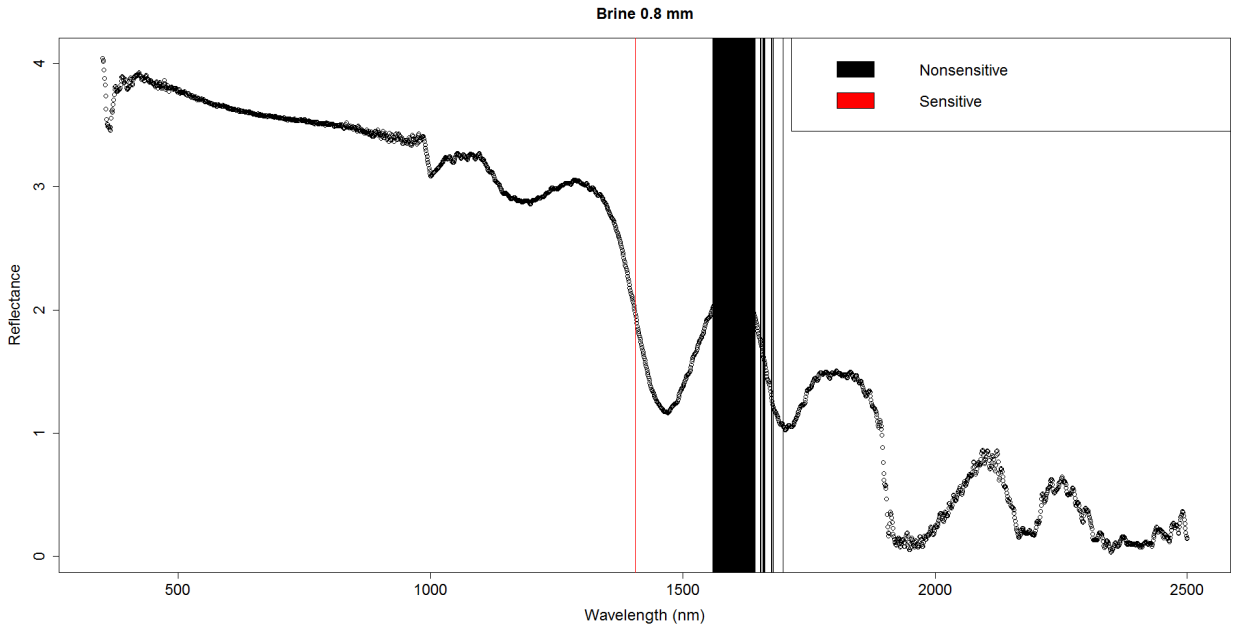

Figure 4.27 Wavelengths with most significant repetition (23.3 percent brine, 0.8 mm)

The red line in figure 4.27 theoretically represents a wavelength that is most sensitive to changes in the brine concentration, while the wavelengths identified in black should be the opposite, the portion of the curve least sensitive to the effects of brine concentration (i.e., the peak remains relatively constant).

The relationships established by analyzing each film thickness did not seem to be very similar, a signifier of the dominating effect of changing water volume thicknesses on spectral reflectance interpretation. The selected wavelengths for the 0.8-mm, 1.6-mm, and 3.6-mm brine solutions were slightly different when tested for replication after extraction of matching points of similar material thicknesses. The resultant data frames of successfully repeated wavelengths were around 1400 for the 0.8-mm film, 1500 for the 1.6-mm film, and 2100 for the 3.6-mm film.

These different successful wavelengths suggest the possibility of multiple volumetric dependent correlations for concentration analysis.

The minimum application thickness recordable in the lab with the established equipment was only 0.8 mm, a thickness greater than the estimated maximum for a well-maintained winter roadway. Therefore, the 0.8-mm relationships were of most concern during the field testing phase. For consistency, other film thicknesses were still tested to determine whether the relationships held valid at all volumetric analysis points. The matched pairs for film thickness revealed significant pairing of the 1820-nm wavelength with wavelengths at 1554 nm, 1555 nm, and 1556 nm (see table 4.7).

Table 4.7 Brine wavelength pairs successful regardless of film thickness

Wvl1	Wvl2	slope	R2	y0	y1	y2	y3	y4
1821	1552	-0.00412	0.914939	0.902327	0.881069	0.859307	0.817814	0.813776
1820	1554	-0.00379	0.875204	0.879718	0.862394	0.851986	0.800835	0.800114
1820	1555	-0.00362	0.873141	0.870093	0.851597	0.845217	0.794945	0.793284
1820	1556	-0.00351	0.864103	0.863125	0.843528	0.840255	0.789643	0.788113

These points were some of the points that will face extra scrutiny during field testing to determine whether the relationship holds true for film thicknesses of less than 0.8 mm and a continuation of a film thickness-independent identifier of brine presence.

Analysis of varied beet-only solutions were conducted to isolate the indicators solely from changing beet concentration. Visually, the addition of beet juice made a stark visual difference (e.g., the solution became darker, redder in color, and less transparent), as shown previously in figure 4.10. A significant change in the visual spectrum was expected to be

produced, as red beet carbohydrate was added because of suppression of the green and blue visual wavelengths. The most repeated wavelength values are shown in table 4.8.

Table 4.8. 3.6-mm beet highest frequency wavelength (nm) for Test 1 (January 24th)

16-Feb	22 mL
Wvl (nm)	Freq
1920	1706
2069	1672
592	1646
608	1646
602	1643
622	1642
593	1641
607	1641
619	1641
620	1641
598	1640
609	1640
618	1640

The 3.6-mm sample of beet extract resulted in the most repeated points occurring at the 1920-nm and 2069-nm wavelengths. However, the majority of the top 20 repeated wavelengths lay in the "orange" visual spectrum (590-625 nm), directly between the yellow and red spectrum. The domination of red reflectance was expected because the carbohydrate beet juice is reddish-black in coloring. A similar procedure was repeated for the 1.6-mm and 0.8-mm samples.

The addition of salt to the beet juice relationships was not evidenced when the 20 most common points were analyzed. The effects of the beet juice still dominated the visual spectrum and continued to be the greatest representation in change of concentration. At a solution thickness of 3.6 mm, the beet-brine relationships with increasing concentration seemed to be most predominant in the yellow spectrum (565 – 590 nm); however, beyond the top 20

frequencies it continued its coverage of the visual spectrum. Reducing the application thickness created surprisingly little difference between the repeated wavelengths.

Chapter 5. Results

5.1 Brine

Using the brine relationships established in the lab setting, where the 1406- to 1408-nm wavelengths compared with the 1560- to 1640-nm wavelengths, produced usable relationships to demonstrate changing sodium chloride concentration. Additionally, the pairs surrounding 1820 nm and 1855 nm were generated as usable points regardless of deicer amount applied in the lab. However, with the thinner applications done in the field, these pairs indicated that the statistical differences were too small for analysis in field use. Of the available brine points, the 1560- to 1640-nm wavelengths were broken down from 1560 to 1590 iterated by 1, and the graphs are spaced out in gaps of 5 nm to show how the relationship was either maintained or changed at the corresponding pairs. Sets of four different pairs and a corresponding ANOVA were conducted for the different types of comparison, shown in this section. For the lab setting, six sets of boxplots were produced to show changes in reflectance (see figure 5.1).

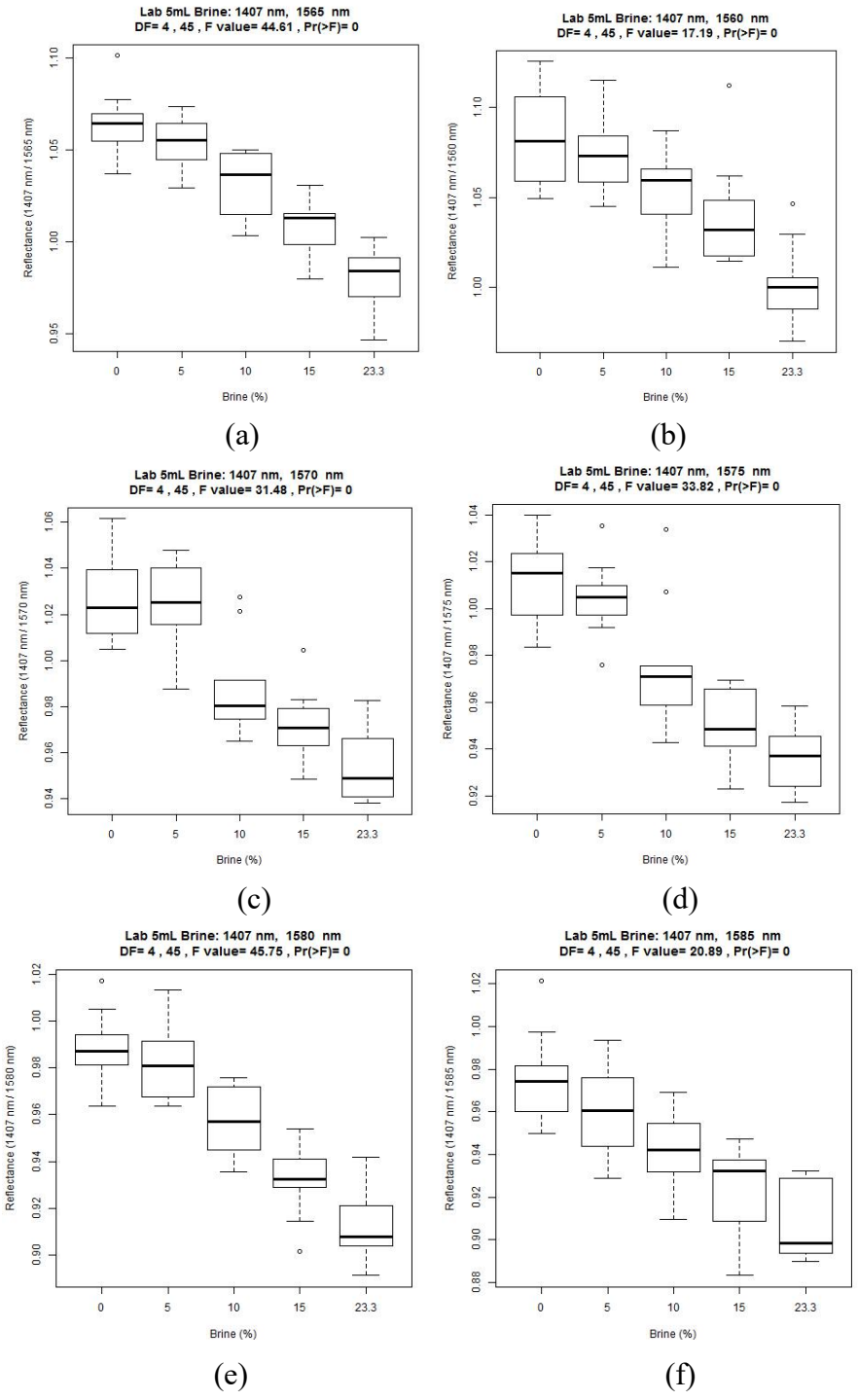

Figure 5.1. Lab-generated brine boxplots (a) through (f)

The largest divergence in band math values seemed to occur at the transition from 5 percent saline to 10 percent saline, as seen in figure 5.1c and figure 5.1d.

5.2. Beet-Brine

Identification of beet-brine relationships in the lab revealed a litany of relationships, mainly due to the visual impact of the changing beet-brine concentration. The changes in the visual spectrum made the range of working relationships vast, with approximately 1700 matching pairs for each wavelength located in the visual spectrum as established by lab-generated data. Of the analyzed relationships, the graphs presented here utilize the most commonly found wavelength of 418 nm, which was then compared to the rest of the wavelengths from 350 to 2500, iterating by 25 nm. The section with the best working relationship, boxplots that had most statistically significant difference as found by ANOVA, showed very strong relationships between 525 nm to 1350 nm and an assortment of four spread out by 100 nm, as shown in figure 5.2.

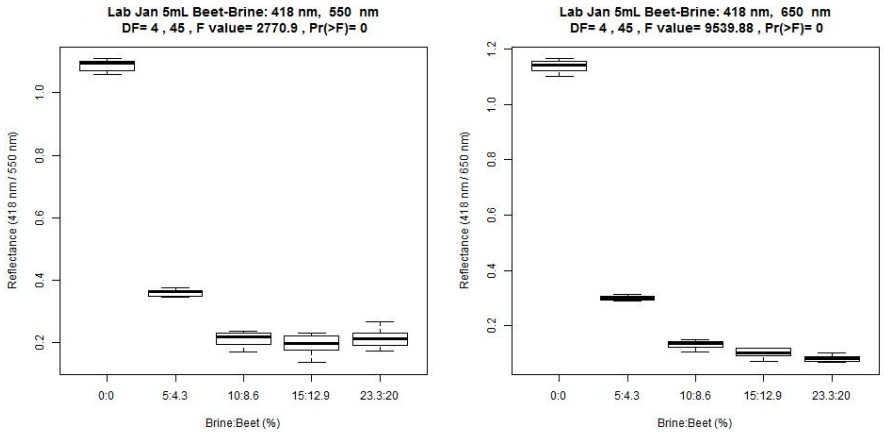

(a)

(b)

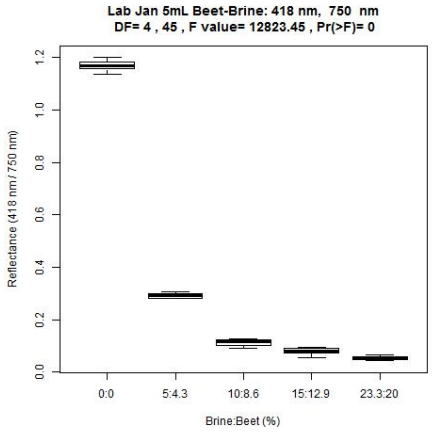

(c)

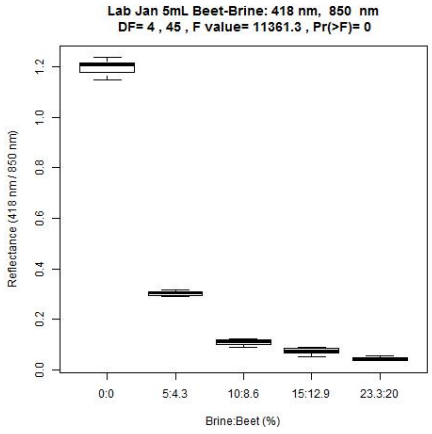

(d)

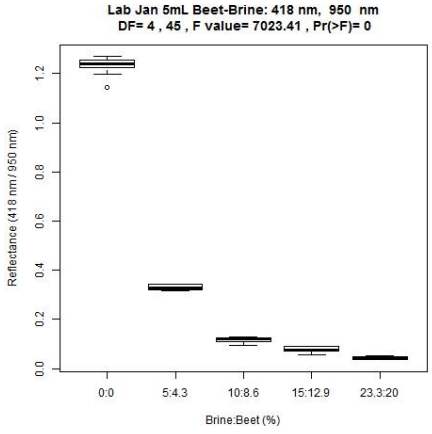

(e)

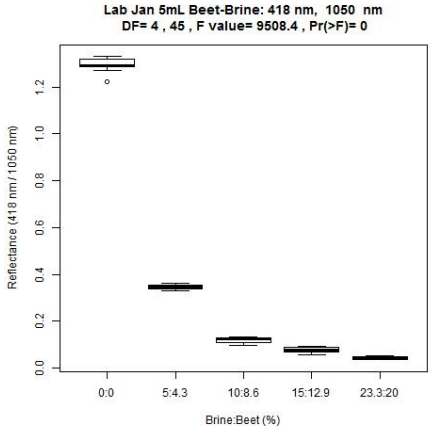

(f)

Figure 5.2. Lab-generated beet-brine boxplots (a) through (f)

The ANOVA test for 418 nm compared to 850 nm showed a statistically significant difference between concentrations of deicing compound [$F(4,45) = 11361$, $p < 0.001$] in the lab

setting. A pairwise comparison using t-tests showed that all concentrations were statistically significantly different.

Chapter 6. Discussion and Conclusion

The goal of this research project was to explore the feasibility of utilizing spectral imaging hardware to establish relationships that could represent the presence and concentration of deicing materials applied to winter roads. To that end, the methods and data generated for this project represent a first step in the development of an objective method to detect and quantify chlorides and related solutions in roadway environments.

Initially, the identification and analysis of deicing compounds, most notably sodium chloride and the carbohydrate red beet juice, seemed relatively straightforward. Our research began with the appraisal of current applications of remote sensing, which identified a similar project that had addressed the salinity of soils as it relates to plant health. Our experimentation started in a lab setting in order to maximize controlled variables and slowly expanded from that point, adding more uncertainties that would be realistically found in real-world applications of the technology. In the lab setting, background, lighting, temperature, runoff, film thickness, and compound were held constant. Utilizing these methods, the older relationship (salt index) was tested, and new successful relationships were discovered and developed. In addition, general knowledge of the spectral imaging reflectance curves of different materials located on winter roadways was expanded.

The new relationships used key wavelengths that experienced a statistically significant change as concentration was adjusted. This involved exploring the application of band math and the development of new spectral analysis techniques to establish trends in which the "significant" points of a curve (the peaks and valleys of the curve) were compared to one another.

A possible oversight encountered during analysis of the peaks and valleys was that some of the valleys approached or even exhibited non-reflectance. The reason a reflectance value of zero is problematic is that adding or changing surface materials, in other words possibly increasing the absorbance of a wavelength that is already at or near 0, might be muted or completely undetected as a change response at that particular wavelength. Because changes in reflectance at wavelengths in which the value is already near zero might not be detected at all by the spectral equipment currently available, the range of wavelengths used for relationship analysis was expanded to every nm available, from 350 to 2500 nm. This approach eliminated the need for offsetting and normalization of numerous consistent and repeatable trends for both the brine and beet-brine mixtures. The differences for beet-brine mixtures in a lab setting were much more significant than those developed for purely brine mixtures. The brine mixtures utilized NIR as key wavelengths and had slight overlap when graphed as boxplots, whereas the beet-brine mixtures utilized the visual spectrum and successfully created linear relationships with up to 1700 of the other wavelengths available.

A major difficulty experienced in this research was the deleterious effects of water on NIR wavelengths. As the deicing compound accomplished its purpose, melting ice, water was created and began to pool on the application site. At certain thicknesses, types, and conditions, water and ice have extremely low reflectance values (i.e., ice and water absorb light and can prevent the identification of other materials contained in solution). Adding salt to water to make a brine results in absorption features and depressed reflectance in the NIR range, making reflectance either impossible to see or massively muting key brine signatures. The best solution for seeing parts of the NIR curve for water was to decrease the film thickness; however, in doing this we discovered that the minimum thickness creatable in the laboratory setting was 0.8 mm

and that maintaining that thickness was a challenge. The thickness could theoretically be decreased further by creating surface striations on the container. However, the uneven visual markings made this an undesirable solution, and the research had to be limited to a minimum thickness of 0.8 mm. Other dish materials were tested to host the liquid solutions that wouldn't interfere with spectral radiance values; however, thinner applications were not successfully achieved.

Limitations also included accurately creating lab conditions that would mimic field conditions. The first steps in lab testing were a form of proof of concept, pouring liquid until a petri dish had full surface coverage, which turned out to be 22 mL of solution or a 3.6-mm-thick solution. This starting point revealed many of the problems associated with absorptive properties of water, the obvious solution being to use less water. The film thickness could be decreased to a minimum of 5 mL or 0.8 mm before the liquid film would adhere to one side of the petri dish, eliminating the possibility of full surface coverage. An intermediary point of 10 ml or 1.6 mm was used to monitor how changes in film thickness would affect the spectra. The resulting spectra showed more of the NIR spectral curve as volume decreased. However, even at the smallest volume repeatable in the lab, the volume of liquid and thereby mg/cm^2 of salt applied was much greater than the volumes AKDOT&PF Northern Region stated that it applied. Techniques to achieve smaller films were explored by changing petri materials and creating surface striations to prevent the liquid from adhering to itself, with limited success. The best solution was to fabricate an iced road segment that would allow the application of amounts similar to AKDOT&PF's winter roadway applications.

Fabrication of a lab-based asphalt pavement road was accomplished by using a black PVC endcap to house the simulated winter road. An asphalt pavement core was fabricated by

using AKDOT&PF specifications and gyratorally compacting, coring, and cutting it into a layer that would fit into the PVC end caps. The simulated roads were a great success in terms of asphalt pavement spectral reflectance; small, easily modifiable roadways, and a controlled area. A specified amount of liquid water could then be applied, and the specimens could be frozen for specific ice thicknesses. However, a problem arose during testing of the deicing compounds. Maintaining the ice layer after fabrication was problematic. The lab research required measuring the reflectance of material in a building on the upper campus at UAF, and by the time the material had been aligned, referenced, applied, and recorded, the surface ice would have begun to melt not because of deicing applications but because of temperature fluctuations. This highly accelerated melt proved impossible to rectify without access to a walk-in freezer that would provide single occupants a few extra hours and internal power outlets. Such facilities were unavailable at the time of the research but would have been extremely beneficial for lab testing by allowing the use of a relevant background material instead of petri dishes.

Only linear relationships and ratios were explored in the final automated pair comparisons. Even with this simplification, the vast number of pairs required two to three days of computation. The resulting outputs, however, still produced many successful relationships. Out of the wavelengths available, every point from 350 nm to 2500 nm, pairs were collected that showed a linear trend, either positive or negative, as concentrations changed. For some sampled data sets the number of paired wavelengths that created successfully linear trends exceeded two million. Of those many points, different methods were used to collate and cull the available pairs. The best course of action was to repeat the testing procedure on a new set of the same values, thereby confirming repeatability of the procedure and relationships.

The automated peak and valley analysis produced R-squared values, slope values, and counted how many times a given wavelength was repeated (i.e., a larger R squared that produces a better linear trend may not always be a good qualifier if a more parabolic trend is a better representation). A large slope could theoretically provide more sensitivity to change, and whichever wavelength was repeated the most would be the wavelength most sensitive to changes in concentration. All these procedures resulted in numerous wavelengths that worked in a lab setting under idealized lighting conditions, constant temperature, and known values to accurately identify changes in concentration.

The approach that promised the highest likelihood of success was to select the points that had the highest rate of repetition, theoretically representing the wavelengths that would exhibit the greatest sensitivity to changes in concentration and volume. The wavelengths that had the highest number of matching points to their curve that produced a linear trend were then statistically analyzed. For the samples in the lab setting the relationships were extremely strong. There was statistically significant difference between each change in concentration and a consistent trend for both the brine and beet-brine compounds. While there were numerous sets of points, sometimes even over 1000 for beet-brine in particular, the results had to be culled to reasonable standards. Since brine had a range of only about 90 consecutive points, the four that best visually appeared to represent the brine relationship at an even 5-nm spacing were shown in this paper. Beet-brine solutions, having a much larger range of points available, were instead iterated at 100 nm to show changes in accuracy.

Both relationships proved to be highly accurate in a lab setting. Beet-brine relationships were a lot stronger and numerous than brine relationships in the lab setting, likely because of the red coloring of the beet-derived concentrate.

This research established that changes in concentration of deicers, specifically brine and beet-brine, can be accurately measured and are statistically significantly different at different concentrations, with consistent trends being identified in a controlled lab setting. As more variables are added or changed, the lab-based relationships become less effective. Further research could explore which specific elements are the cause, whether it is the changing temperature, application migration, background instability due to melting and changing ice structure, background uncertainty due to asphalt pavement, or perhaps the equations themselves. This research specifically limited its scope to only two variables (i.e., concentration and volume) in the analysis, but it presents a framework for analyzing winter roadway maintenance efforts. New sets of spectra specific to the components of winter roadways were also produced and analyzed.

The ability to identify the concentration and location of brine and beet deicers with spectral imaging has considerable value for practical applications such as winter maintenance and future research into topics such as deicer dispersion and tracking. Monitoring the concentration of anti-icers and deicers would allow real-time monitoring to ensure adequate deicing concentrations. As a result, road maintenance crews could avoid conditions in which a deicing chemical became too diluted and could not function as intended, possibly refreezing the surface ice and making winter roadways more dangerous. Accurate measurements of anti-icing and deicing chemicals would facilitate safer winter roadways, as well as more effective use of state materials intneded to maintain safety and reduce operating budgets. The ability to track and locate surface presence would also be valuable for tracking migration and learning more about the methods by and quantities at which these chemicals migrate within and off the roadway. This

is of particular interest because salts and carbohydrates can harm wildlife and some infrastructure.

Phase 2 of this project will focus on field-based data and how to extend the methods developed in Phase 1 into environmental settings that are perhaps more varied. Future research could also improve the laboratory methods by employing the use of a cold room to aid in the fabrication of samples, as well as obtaining the spectra of the specimens to avoid melting of thin film thicknesses.

References

Alberta Infrastructure and Transportation. 2006. Road Weather Information System (RWIS) Deployment Plan for Alberts's National Highway System (NHS).

American Public Health Association (1976) "Standard Methods for the Examination of Water and Waste Water," (1976). 14th ed., 1976. Washington, DC.

Asfaw, E., Suryabhagavan, K., & Argaw, M. (2016, May 19). Soil salinity modeling and mapping using remote sensing and GIS: The case of Wonji sugar cane irrigation farm, Ethiopia. Retrieved December 15, 2017, from https://www.sciencedirect.com/science/article/pii/S1658077X16300042#b0035

City of Fairbanks (n.d.). Public Works Department. Retrieved December 15, 2017, from http://www.fairbanksalaska.us/departments/public-works/

Conger, S.M. 2005. Winter highway maintenance: a synthesis of highway practice. NCHRP Synthesis 344, National Research Council, Washington, D.C.

Corsi, S. R., Geis, S. W., Bowman, G., Failey, G. G., & Rutter, T. D. (2008, October 31).Aquatic Toxicity of Airfield-Pavement Deicer Materials and Implications for Airport Runoff. Retrieved December 15, 2017, from http://pubs.acs.org/doi/pdf/10.1021/es8017732

CTC & Associates, (2008). *Limitations of the Use of Abrasives in Winter Maintenance Operations.* Prepared for the Wisconsin Department of Transportation. 2008.

Dolce, C. (2017, December 12). Snow Has Already Been Recorded in All 50 States, and It Isn't Even Winter Yet. Retrieved December 15, 2017, from https://weather.com/storms/winter/news/2017-12-12-snow-50-states-winter-2017-18

ECOSTRESS Spectral Library (2018, February 2). Jet Propulsion Laboratory. Retrieved from https://speclib.jpl.nasa.gov/

Fay, L., M.Sc, Honarvarnazari, M., Ph.D., Jungwirth, S., M.Sc., Muthumani, A., M.Sc., Cui, N., Ph.D., & Shi, X., Ph.d., P.E. (2015, June). Manual for Environmental Best Practices for Snow and Ice Control (Proj.). Western Transportation Institute. http://clearroads.org/wp-content/uploads/dlm_uploads/Manual_ClearRoads_13-01_FINAL.pdf

Fay, L., Volkening, K., Gallaway, C. and Shi X., in Proceedings (DVD-ROM) of the 87th Annual Meeting of Transportation Research Board (held in Washington D.C., January 2008), eds. Transportation Research Board, (2008), Paper No. 08-1382.

FHWA, 1996

Federal Highway Administration (2017a) *Snow and Ice*. Retrieved December 10, 2017, from https://ops.fhwa.dot.gov/weather/weather_events/snow_ice.htm

Federal Highway Administration (2017b). *How Do Weather Events Impact Roads?* Retrieved February 2, 2019 from https://ops.fhwa.dot.gov/weather/q1_roadimpact.htm

Federal Highway Administration. *Manual of Practice for an Effective Anti-Icing Program*. (2012, February 08). Federal Highway Administration Retrieved December 15, 2017, from https://www.fhwa.dot.gov/publications/research/safety/95202/005.cfm

GIS Geography, (2018). *What is NDVI (Normalized Difference Vegetation Index)?* Retrieved from https://gisgeography.com/ndvi-normalized-difference-vegetation-index/ June 20, 2018.

IHS (2014, February 24). The Economic Costs of Disruption form a Snowstorm Retrieved December 12, 2017, from https://www.highways.org/wp-content/uploads/2014/02/economic-costs-of-snowstorms.pdf

Kuemmel, D. A., & Hanbali, R. M. (1992, June 1). Accident Analysis of Ice Control Operations (Rep.). Retrieved December 13, 2017, from The Salt Institute website: http://www.trc.marquette.edu/publications/IceControl/ice-control-1992.pdf

Lysbakken, K.R., and Stotterud, R. "Prewetting Salt with Hot Water," PIARC XII International Winter Roads Congress, Sistriere, Italy, 2006

McClellan, T., Boone, P. and Coleman, M. 2009. Maintenance Decision Support System (MDSS): Indiana Department of Transportation (INDOT) Statewide Implementation, Final Report. Indiana DOT.

Monteleone, D. (2012). Maintenance & Operations. Retrieved December 15, 2017, from http://dot.alaska.gov/stwdmno/

National Academies of Sciences, Engineering, and Medicine. 2007. *Guidelines for the Selection of Snow and Ice Control Materials to Mitigate Environmental Impacts*. Washington, DC: The National Academies Press. https://doi.org/10.17226/23178. Prepared for the NCHRP Project 6-16.

Nixon, W. A., Kochumman, G., Qiu, L., Qiu, J., & Xiong, J. (2007, May). Evaluation of Using Non-Corrosive Deicing Materials and Corrosion Reducing Treatments For Deicing Salts (Rep. No. IHR Technical Report #463). IIHR - Hydroscience & Engineering.

Ontario Ministry of Transportation. "Making Sand Last: MTO Tests Hot Water Sander" Road Talk, Vol. 14, No. 2, Summer, 2008.

Roads & Bridges, (2017, May 24). *WINTER MAINTENANCE: Snow removal cost Anchorage*. Retrieved December 15, 2017, from https://www.roadsbridges.com/winter-maintenance-snow-removal-cost-anchorage-alaska-millions-more-winter-previous-years

Schuckman, Karen (n.d.). *Band Math*. Retrieved from John A Dutton e-Education Institute, PennState College of Earth and Mineral Sciences: https://www.e-education.psu.edu/geog480/node/524

Staples, J.M., Gamradt, L., Stein, O., Shi, X., 2004. Recommendations for winter traction materials management on roadways adjacent to bodies of water. Montana Department of Transportation. FHWA/MT-04-008/8117-19. http://www.mdt.mt.gov/research/docs/research_proj/traction/final_report.pdf

Sumsion, E. S., & Guthrie, S. W., Ph.D. (2013). Physical and Chemical Effects of Deicers on Concrete Pavement: Literature Review (Rep. No. UT-13.09). Brigham Young University Department of Civil and Environmental Engineering.

Synthesis of Best Practices, Road Salt Management. (2003). Transportation Association of Canada. Retrieved from http://www.tac-atc.ca/english/resourcecentre/readingroom/pdf

Transportation Performance Management. (2017, June 27). Federal Highway Administration Retrieved December 15, 2017, from https://www.fhwa.dot.gov/tpm/about/goals.cfm

USDOT (2012). *Best Practices for Road Weather Management*. Retrieved August 17, 2018. http://www.ops.fhwa.dot.gov/publications/fhwahop12046/rwm07_colorado1.htm

Vaa, T. "Implementation of New Sanding Method in Norway." Transportation Research Circular Number E-C063, 2004. http://onlinepubs.trb.org/onlinepubs/circulars/ec063.pdf

Williams, A. L., Stensland, G. J., Peters, C. R., & Osborne, J. (2000). Atmospheric Dispersion Study of Deicing Salt Applied to Roads (Rep.). Champaign, Illinois: Illionois State Water Survey Atmospheric Environment Section.